CZECH TECHNICAL UNIVERSITY IN PRAGUE
FACULTY OF MECHANICAL ENGINEERING
DEPARTMENT OF ENVIRONMENTAL ENGINEERING

CFD MODELLING AND SIMULATION OF A CENTRIFUGAL FAN

MASTER THESIS

TAO JIANG   3 – EE – 2021

MASTER'S THESIS ASSIGNMENT

I. Personal and study details

Student's name:	**Jiang Tao**	Personal ID number:	**483956**
Faculty / Institute:	**Faculty of Mechanical Engineering**		
Department / Institute:	**Department of Environmental Engineering**		
Study program:	**Mechanical Engineering**		
Branch of study:	**Environmental Engineering**		

II. Master's thesis details

Master's thesis title in English:

CFD Modelling and Simulation of a Centrifugal Fan

Master's thesis title in Czech:

CFD modelování a simulace radiálního ventilátoru

Guidelines:

Create a CFD model of the centrifugal fan type RFE 200-L produced by ALTEKO company. Use the Multiple Reference Frame (MRF) method available in ANSYS Fluent for the problems which involve rotating parts (e.g. a fan wheel). Compare the results from your own CFD simulations with the fan performance curves provided by ALTEKO.

Bibliography / sources:

Zelenský P., Barták M., Zavřel V., Zmrhal V., Krupa R. Numerical Analysis of Air Flow in a Modular Fan Unit Using CFD Simulation. In: Proceedings of CLIMA 2019 Congress. Les Ulis Cedex A: EDP Sciences, 2019. E3S Web of Conferences. vol. 111 - 2019. ISSN 2267-1242.
Gullberg P., Sengupta R. Axial Fan Performance Predictions in CFD: Comparison of MRF and Sliding Mesh with Experiments. In: Proceeding of the 11th European Conference on Turbomachinery Fluid Dynamics and Thermodynamics, Istanbul, Turkey, 2011.
ANSYS Fluent Documentation. ANSYS, 2019.

Name and workplace of master's thesis supervisor:

Ing. Martin Barták, Ph.D.,   Department of Environmental Engineering,   FME

Name and workplace of second master's thesis supervisor or consultant:

Ing. Petr Zelenský, Ph.D.,   Department of Environmental Engineering,   FME

Date of master's thesis assignment: **30.04.2021**   Deadline for master's thesis submission: **04.07.2021**

Assignment valid until: _____

_____	_____	_____
Ing. Martin Barták, Ph.D.	doc. Ing. Vladimír Zmrhal, Ph.D.	prof. Ing. Michael Valášek, DrSc.
Supervisor's signature	Head of department's signature	Dean's signature

III. Assignment receipt

The student acknowledges that the master's thesis is an individual work. The student must produce his thesis without the assistance of others, with the exception of provided consultations. Within the master's thesis, the author must state the names of consultants and include a list of references.

_____	_____
Date of assignment receipt	Student's signature

Summary

The thesis topic falls into the field of CFD modelling and simulation of fluid flow in devices with rotating parts. Specifically, the aim of this work was to simulate the performance curve (P-V) of the radial fan type RFE 200-L produced by ALTEKO company. The model was created in ANSYS SpaceClaim 3D modelling software and the simulations were performed in ANSYS Fluent. The rotation of fan impeller was simulated using the multiple reference frame (MRF) method. In general, a fan performance curve shows total pressures and volumetric flow rates delivered by the fan at constant speed of rotation. Therefore, the fan model was set to different operating conditions determined by the static gauge pressure at the model outlet. These gauge pressures may represent various pressure losses of a virtual duct system connected to the fan. Five operating points were simulated based on the gauge pressure at the model outlet set to 0, 100, 200, 300 and 350 Pa. For each operating point, the fan total pressure and the flow rate of standard air (density 1.2 kg/m^3) were evaluated. The simulated performance curve was compared with the measured curve provided by the fan manufacturer. The simulated curve is very close to the measured one up to the fan total pressure of 250 Pa. For total pressures higher than 250 Pa, the simulated curve is lower than the measured one. The maximum total pressure estimated from the trend of simulated curve could be approximately 400 Pa while the measured maximum total pressure is 500 Pa.

Souhrn

CFD modelování a simulace radiálního ventilátoru

Téma práce patří do oboru CFD modelování a simulací proudění v zařízeních s rotujícími prvky. Konkrétně cílem této práce bylo nasimulovat výkonovou charakteristiku (P-V) radiálního ventilátoru typu RFE 200-L vyráběného firmou ALTEKO. Model byl vytvořen v softwaru pro 3D modelování ANSYS SpaceClaim a simulace byly provedeny v prostředí ANSYS Fluent. Rotace oběžného kola ventilátoru byla simulována metodou vícenásobného souřadnicového systému (MRF). Obecně výkonová charakteristika ventilátoru ukazuje celkový tlak a objemový průtok dodávaný ventilátorem při konstantních otáčkách. Proto byl model vystaven různým provozním podmínkám určeným statickým přetlakem na výstupní hranici modelu. Tento přetlak může reprezentovat různé tlakové ztráty ve virtuálním potrubním systému připojeném k ventilátoru. Bylo nasimulováno pět provozních bodů určených statickým přetlakem na výstupu z modelu 0, 100, 200, 300 a 350 Pa. Pro každý provozní bod byl vyhodnocen celkový tlak ventilátoru a průtočné množství standardního vzduchu (hustota 1,2 kg/m^3). Nasimulovaná výkonová charakteristika byla porovnána s naměřenou charakteristikou, kterou poskytl výrobce ventilátoru. Nasimulovaná charakteristika leží velmi blízko k naměřeným hodnotám až do celkového tlaku 250 Pa. Pro vyšší celkové tlaky než 250 Pa je nasimulovaná charakteristika nižší než naměřená. Zatímco z trendu nasimulované charakteristiky lze odhadnout maximální celkový tlak cca 400 Pa, naměřený maximální celkový tlak je 500 Pa.

Declaration

I declare that this diploma thesis entitled "CFD Modelling and Simulation of a Centrifugal Fan" is my own work performed under the supervision of Ing. Martin Bartak, Ph.D., with the use of the literature presented at the end of my diploma thesis in the list of references.

In Prague 02.07.2021

…………………
Tao Jiang

Acknowledgments

I deeply appreciate my supervisor Ing. Martin Bartak, Ph.D., for his constant encouragement and guidance during my master's thesis. Regarding to his wonderful lectures, such as Aerodynamic of Ventilation and the Heat Transfer, I understood the fluid and heat transfer in microcosmic aspect, and these knowledge was very useful during the thesis writing. Furthermore, under his guidance and patiently explanation, I learned how to use the software ANSYS, and this skill will be an advantage in my future career.

Secondly, my deepest gratitude also goes to Ing. Petr Zelensky, Ph.D., for his consultations and guidance during the modeling process. Without his consistent instructions, the model could not be created and the problem could not be solved.

At last, I would like to express my sincere thanks to Department of Environment Engineering, my classmates and all the teachers who have taught and helped me.

Contents

Nomenclature

Latin letters

$\vec{A}$	Surface area vector (m^2)
A_i	Facet area of a cell (m^2)
$\hat{a}$	Unit direction vector (-)
$\vec{F}$	External body force (N)
$\vec{g}$	Gravitational acceleration (m/s^2)
k	Turbulent kinetic energy (m^2/s^2)
$\vec{r}$	Position vector (m)
P	Static pressure (Pa)
t	Time (s)
u^+	Dimensionless velocity (-)
u_τ	Friction velocity (m/s)
$\vec{u_r}$	Velocity of the moving frame relative to the inertial reference frame (m/s)
V	Volume (m^3)
$\vec{v}$	Velocity vector (m/s)
y	Distance from the wall (m)
y^+	Dimensionless wall distance (-)

Greek letters

ρ	Fluid density (kg/m^3)
∇	Hamilton operator (1/m)
ε	Turbulent energy dissipation rate (m^2/s^3)
$\vec{\omega}$	Angular velocity (rad/s)
τ_w	Wall sheer stress (Pa)
μ_t	Turbulent viscosity (Pa·s)
μ	Dynamic viscosity (Pa·s)
ν	Kinematic viscosity (m^2/s)

List of Abbreviations

CFD   Computational Fluid Dynamics

CAD   Computer Aided Design

EWT   Enhanced Wall Treatment

RPM   Revolution Per Minute

MRF   Multiple Reference Frame

PISO   Pressure-Implicit with Splitting of Operators

SC   SpaceClaim

SM   Sliding Mesh

SIMPLE   Semi-Implicit Method for Pressure Linked Equations

STEP   Standard for the Exchange of Product Data

1.Introduction

With the development of the technology, methods and tools for the equipment design are constantly being innovated. Besides standard design methods, other alternative approaches for design are increasingly popular, such as simulations. The main purpose of using simulation methods in equipment's or system's design process is to reduce the costs for design and operation. Secondly, it is also possible to modularize a complex system in divide, and then simulate each module separately, thereby reducing the workload and increasing the fault tolerance of the system optimization. Thirdly, the simulation provides inaccessible information of the equipment or system during the design process, which can be used to propose and optimize the equipment or system. In total, affordability, convenience and reliability are important considerations for simulation.

The above mentioned advantages apply also to the computational fluid dynamics (CFD) modelling and simulation. Nowadays, the CFD technique is widely used in the design field. It can provide detailed flow information like pressure, temperature, velocity and other quantities in the solved domain. Therefore, the CFD simulations help to understand better the hidden interactions of the flow. This ability of CFD simulations is demonstrated in this project: detailed information of the flow in the fan chamber of the centrifugal fan can be analyzed both numerically and visually.

The purpose of this work is to create a CFD model of the centrifugal fan type RFE200-L produced by ALTEKO. The Multiple Reference Frame (MRF) method available in ANSYS Fluent is used to simulate the model. The results of CFD simulations with the created model are compared to the measured fan performance curves provided by ALTEKO.

2. Centrifugal fans

A fan can be considered as an air pump, in which the impeller works on air to create a pressure difference and to cause air flow. The static and kinetic energy can be transmitted proportionally with the air flow according to the fan types.

In general, fans are classified as centrifugal or axial according to the direction of airflow through the impeller. With different impeller design and fan housing design, the centrifugal fan can be categorized as radial, forward-curved, backward-inclined and backward-curve [1]

All fans produce pressure and flow through the rotating blades of impeller to impart the kinetic energy to the air by changing of the air velocity. For centrifugal fans, the velocity change is in the tangential and radial velocity components, otherwise, in the tangential and axial velocity components for the axial fans.

In centrifugal fan, the centrifugal force is created by rotating air column contained between the blades and pressure is produced by impeller. The kinetic energy imparted to the air by virtue of air velocity leaving the impeller. This velocity consists of the rotative velocity of the impeller and airspeed relative to the impeller. When the blades in impeller are backward-curved, these two velocities are noncumulative, oppositional the velocities are cumulative when the blades are forward-curved. The basic structure of centrifugal fan is shown in Fig. 1.
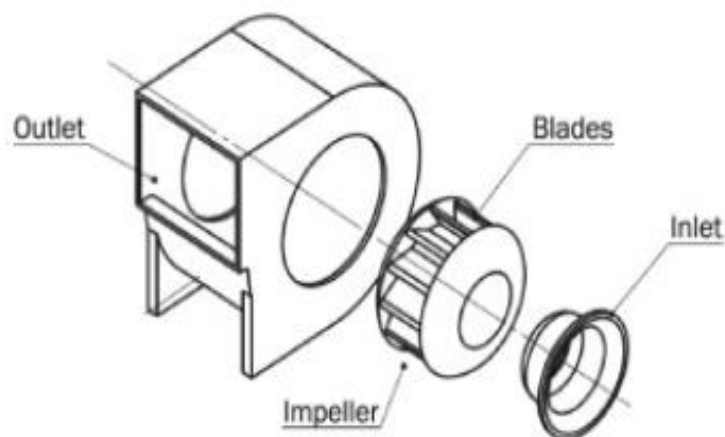

Fig. 1 - Centrifugal fan components [7]

Centrifugal fans are widely used for ventilation, dust exhaust and cooling of factories, mines, tunnels, cooling towers, vehicles, ships and buildings; ventilation and induced air for boilers and industrial furnaces; and for air conditioning equipment and household appliances，such as cooling and ventilation etc.

Over the last 20 years centrifugal fans with backward curved blades have become more common within air handling. They are normally larger for the same volume and pressure characteristics and are a little more complicated to construct, so more expensive [2]. Despite the cost disadvantage, they have become more popular in air handling units because they are more efficient than forward curved centrifugal fans.

In order to make the centrifugal fan work better, it is extremely important to know its working characteristics. One of the most important indicators of characteristic of centrifugal fan is the P-V performance curve. The common method to achieve the P-V performance curve is using equipment and make experiments in laboratory.

The performance curves of centrifugal fans such as power, total efficiency, static efficiency, total pressure and static pressure, relates to the volume flowrate are given in the 2000 ASHRAE System and Equipment Handbook [1]. The highest efficiency of centrifugal fans occurs nearly at 50% of wide opened volume, and this volume has also the good pressure characteristics of centrifugal fans. The power of centrifugal fans reaches maximum near peak efficiency and becomes lower towards free delivery.

3. Computational fluid dynamics (CFD)

Computational Fluid Dynamics (CFD) can analyze and figure out the important features of systems for fluid flow and heat transfer by computational simulation. It is very powerful and widely used in the industrial or non-industrial application areas, for example in aerodynamics of aircraft and vehicles; turbomachinery; electrical and electronic engineering; external and internal environment of buildings etc.

From the 1960s the CFD techniques has been integrated into the design and manufacture of aircraft and jet engines. In 1990s the CFD was widely used in industrial community after the availability of affordable high performance computing hardware and introduction of user friendly interfaces has developed [3]. Recently the design of internal combustion engines, combustion chambers of gas turbines and furnaces were also using the CFD methods. Besides, for predicting drag forces, under-bonnet air flows and the car environment in motor vehicle manufacture the CFD techniques are also indispensable.

The efficiency of the CFD simulation for applications relates to the complexity of geometry of the models; difficulty of the creating of the numerical model, such as the preparation of computational mesh and the simulation setup, and so on. Fortunately, the software tools for the pre-processing of models for the CFD simulation has been significant developed in last decades. It helps the designers or engineers save numerous times in products design or system built i.e. analyze.

CFD is becoming a vital component for designing a industrial products and processes. The advantages of CFD for fluid system design are:

• The system could be studied under hazardous conditions and beyond their normal performance limits.
• The system could be also analyzed where the controlled experiments are difficult or impossible to perform.
• Reduction of lead times and costs of a new design.
• Unlimited level of detail of the results.

The fluid flow problems such presented in this work, can be tackled by CFD code, and structured around the numerical algorithms. All codes contain three main elements, a pre-processor, a solver and a post-processor [3].

Pre-processor

Before numerical simulation in the solver, the model should be numerically prepared and transformed to a suitable form, which can be used by the solver. The pre-processing stage consists of:

- Definition of the model geometry.
- Grid generation.
- Selection of the physical phenomena.
- Definition of fluid properties.
- Specification of appropriate boundary conditions.

Solver

The numerical methods which form the basis of the solver perform the steps below:

- Approximation of the unknown flow variables by simple functions.
- Discretization by substitution of the approximations into the governing flow equations and mathematical manipulations.
- Solution of the algebraic equations.

Post-processor

The results are presented through the data visualization tools, which include:

- Model geometry and grid display.
- Vector plots.
- Line and shade contour plots.
- 2D and 3D surface plots.
- Particle tracking.

3.1. General mathematical background

ANSYS Fluent can provide comprehensive modelling capabilities for problems with various types of flow, such as incompressible, compressible, laminar or turbulent. Steady state or transient state can be analyzed in Fluent. A wide range of mathematical models for transport phenomena is combined with the ability for modelling of complex geometries.

Conservation equations for mass and momentum for all flows can be solved by ANSYS Fluent. An additional equation for energy conservation is solved only when the flow involves heat transfer or compressibility. In this work, the model represents turbulent flow in a fan chamber, thus only the conservation equations of mass and momentum are considered.

There are three distinct streams of numerical solution techniques in solver of CFD simulation:
1) Finite difference methods;
2) Finite volume methods;
3) Spectral methods.

The finite volume method was used in this work. The reason for Finite Volume Method (FVM) is that the Fluent solver is based on it. The whole model was divided into three control volumes i.e. computational cell zones: volume of inlet, volume of rotated impeller, volume of outlet.

3.2. Multiple reference frame (MRF)

In general, ANSYS Fluent solves the equations of fluid flow and heat transfer in a stationary reference frame. However, there are many problems where the equations in moving reference frame should be solved. These problems typically involve moving parts, such as in this work, the rotating impeller with blades is involved. The moving parts present the problem unsteady when viewed from a stationary frame, nevertheless, the flow around the moving part can be modelled as a steady-state problem with respect to the moving frame.

For problems that refer the entire computational domain to a single moving reference frame the single reference frame (SRF) approach is used. SRF can be used only when the geometry meets certain requirements. For more complex geometries, the problem must be broken up into multiple zones, with well-defined interfaces between the zones. The way the interface is handled leads to two approximate steady-state modelling methods for such problems: the multi-reference frame (or MRF) method and the hybrid plane method.

Problems involving multiple moving parts should be modelled with the MRF approach, thus the model must be broken up into multiple cell zones, with interface boundaries separating the zones. The zones contain the moving components can then be solved using the moving reference frame equations (described in chapter 3.2.1), meanwhile the stationary zones can be solved with the stationary frame equations.

At the interfaces between cell zones, a local reference frame transformation is performed to enable flow variables in one zone to be used to calculate fluxes at the boundary of the adjacent zone. The MRF interface formulation will be discussed in chapter 3.2.2.

3.2.1. Equations for a moving reference frame

For a steadily moving frame, the rotational speed is constant. It is possible to transform the equations of fluid motion to the moving frame. It is also possible to run an unsteady simulation in a moving reference frame with constant rotational speed. Besides, the appropriate acceleration terms should be added to the equations of fluid motion, if frame moves with unsteady translational and rotational speeds.
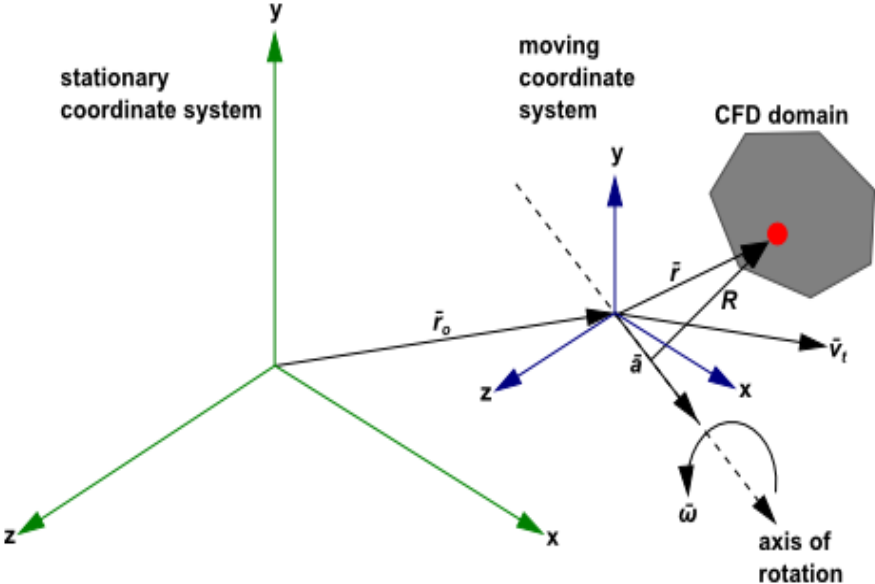

Fig. 2 - Stational and moving frame [4]

As showing in Fig. 2, a coordinate system is translating with a linear velocity $\overrightarrow{v_t}$ and rotating with angular velocity $\vec{\omega}$ relative to a stationary i.e. initial reference frame. The origin of the moving system is located by a position vector $\overrightarrow{r_0}$ from the stationary coordinate system.

The axis of rotation is defined by a unit direction vector $\hat{a}$, such as $\vec{\omega} = \omega\,\hat{a}$.

An arbitrary point in the CFD domain is located by a position vector $\vec{r}$ from the origin of the moving frame.

The fluid velocities are transformed from the stationary frame to the moving frame with accordance to the following relation:

$$\vec{v_r} = \vec{v} - \vec{u_r} \tag{1}$$

$$\vec{u_r} = \vec{v_t} + \vec{\omega} \times \vec{r} \tag{2}$$

Here $\vec{v_r}$ is the relative velocity (the velocity viewed from the moving frame);

$\vec{v}$ is the absolute velocity (the velocity viewed from the stationary frame);

$\vec{u_r}$ is the velocity of the moving frame relative to the inertial reference frame;

$\vec{v_t}$ is the translational frame velocity;

$\vec{\omega}$ is the angular velocity. In addition, both $\vec{v_t}$ and $\vec{\omega}$ can be functions of time.

Generally, the equations can be formulated in two different ways: **1) The relative velocity formulation**. It expresses the momentum equations using the relative velocities as dependent variables. **2) The absolute velocity formulation**. It expresses the momentum equations using the absolute velocities as dependent variables.

The absolute velocity formulation is preferred to be used in where the flow in most of the domain is not moving, such as a fan in a large room. And the relative velocity formulation is appropriate when most of the fluid in the domain is moving, as in this work, a rotating impeller in fan chamber.

3.2.2. Relative velocity formulation

The governing equations of fluid flow in a moving reference frame for the relative velocity formulation can be presented as following.

Conservation of mass:

$$\frac{\partial \rho}{\partial t} + \nabla \cdot (\rho \vec{v_r}) = 0 \qquad (3)$$

Conservation of momentum:

$$\frac{\partial}{\partial t}(\rho \vec{v_r}) + \nabla \cdot (\rho \vec{v_r}\vec{v_r}) + \rho(2\vec{\omega} \times \vec{v_r} + \vec{\omega} \times \vec{\omega} \times \vec{r} + \vec{\alpha} \times \vec{r} + \vec{a}) = -\nabla p + \nabla \cdot \vec{\tau_r} + \vec{F} \qquad (4)$$

Where the $\vec{\alpha} = \frac{d\vec{\omega}}{dt}$ and $\vec{a} = \frac{d\vec{v_t}}{dt}$.

Compare to the general conservation of momentum, the momentum equation contains four additional acceleration terms. Respectively, the first two terms are the Coriolis acceleration ($2\vec{\omega} \times \vec{v_r}$) and the centripetal acceleration ($\vec{\omega} \times \vec{\omega} \times \vec{r}$). These terms appear for both steadily moving reference frame and accelerating reference frame. Respectively, the third and fourth terms are due to the unsteady change of the rotational speed and linear velocity. These two terms will disappear for constant translation and rotational speeds. In other words, the third and fourth terms vanish in this work, when the flow in fan chamber is fully developed.

3.2.3. The MRF interface formulation

The MRF interface formulation depends on the use of the velocity formulation. The interface treatment applies to the velocity and velocity gradients, since these vector quantities change with a change in reference frame, however, the scalar quantities such as pressure, temperature, density and turbulent kinetic energy e.g. do not need any special treatment, thus they pass locally without any changes.

The calculation domain of the MRF model is divided into subdomains, each of which may be rotating and/or translating with respect to the initial frame. The governing equations in each subdomain are written with respect to that subdomain's reference frame. At the boundary between two subdomains, the terms in in the governing equations in one subdomain require values for the velocities in the adjacent subdomain. The schematic diagram is shown as below.
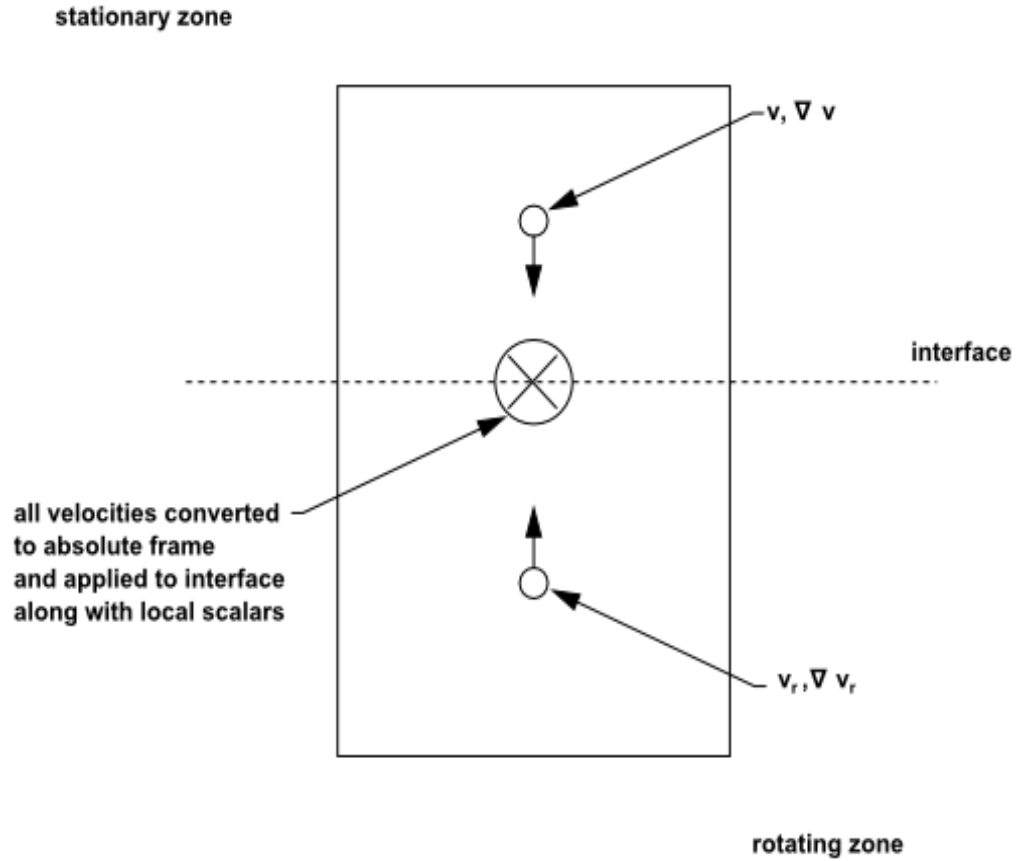
Fig. 3 - Interface treatment for the MRF model [4]

With using of the relative velocity formulation, velocities in each subdomain are computed relative to the motion of the subdomain. Velocities and velocity gradients are converted from a moving reference frame to the absolute inertial frame through the following equations.

For the translational velocity $\vec{v_t}$ using equation:

$$\vec{v} = \vec{v_r} + (\vec{\omega} \times \vec{r}) + \vec{v_t} \tag{5}$$

And for the gradient of the absolute velocity vector using equation:

$$\nabla \vec{v} = \nabla \vec{v_r} + \nabla (\vec{\omega} \times \vec{r}) \tag{6}$$

It should be noted that the scalar quantities such as density, static temperature, static pressure and so on, are simply obtained locally from the adjacent cells.

13

3.3. Realizable k-ε model of turbulence

The two-equation models of turbulence are widely used in industrial CFD. The k-ε model in ANSYS Fluent, with its robustness, economy, and reasonable accuracy for a wide range of turbulent flows, lead its popularity in industrial flow and heat transfer simulations. However, the k-ε model is not widely used in external aerodynamics, because it's insensitivity adverse pressure gradients and boundary layer separated. It usually predict a delayed and reduced separation relative to observations, which can result in overly optimistic design evaluations for flows that separate from smooth surfaces, for example, aerodynamic bodies.

The Realizable k-ε model is relatively recommended in comparison with other variants of the k-ε family. It is necessary to use the k-ε model in combination with either the Enhanced Wall Treatment (EWT- ε) or the Menter-Lechner near-wall treatment. In this work, the Enhanced Wall Treatment is considered and will be described in next chapter.

The two-equation turbulence model, that related to the turbulent kinetic energy -k-T and the rate of dissipation of the turbulent kinetic energy -ε, has three typically variants, the Standard k-ε model by Launder and Spalding [11], the RNG k-ε model by Yakhot and Orszag [12], the Realizable k-ε model by Shih and Loiu [13]. Compare to other two methods, the results of simulations with these models of turbulence do not differ too much form each other, but the Realizable k-ε model by Shih and Loiu [13] with correction on the pressure effects in the boundary layer has the best convergence of the solution. Therefore, the Realizable k-ε model is chosen, it should be noted that this two equation model of turbulence is also commonly be used nowadays et al. [14].

The term "realizable" means that the model satisfies certain mathematical constraints on the Reynolds stresses, consistent with the physics of turbulent flows. Combinate with the Boussinesq hypothesis equation and the eddy viscosity equation, we can obtain the flowing expression for the normal Reynolds stress in an incompressible strained mean flow.

$$\overline{u^2} = \frac{2}{3}k - 2v_t \frac{\partial U}{\partial X} \tag{7}$$

The Boussinesq hypothesis equation presented as:

$$-\rho\overline{u'_i u'_j} = \mu_t \left(\frac{\partial u_i}{\partial x_j} + \frac{\partial u_j}{\partial x_i}\right) - \frac{2}{3}\left(\rho k + \mu_t \frac{\partial u_k}{\partial x_k}\right)\delta_{ij} \tag{8}$$

14

and the eddy viscosity equation is thus:

$$\mu_t = \rho C_\mu \frac{k^2}{\varepsilon} \tag{9}$$

Where the C_μ is a constant equal to 0.09.

The advantage of the Boussinesq hypothesis approach is the relatively low computational cost associated with the computation of the turbulent viscosity μ_t, but also, the disadvantage of the Boussinesq hypothesis is that it assumes an isotropic scalar quantity, which is not strictly true. However, the assumed isotropic turbulent viscosity typically works well for shear flows dominated by only one of the turbulent shear stresses. This covers many technical flows, such as wall boundary layers, mixing layers, jets, and so on.

3.3.1. Transport equation for the Realizable k-ε model

The modeled transport equations for k in the realizable k-ε   model is:

$$\frac{\partial}{\partial t}(\rho k) + \frac{\partial}{\partial x_j}(\rho k u_j) = \frac{\partial}{\partial x_j}[\ (\mu + \frac{\mu_t}{\sigma_k})\frac{\partial k}{\partial x_j}\ ] + G_k + G_b - \rho\varepsilon\ -Y_M - S_k \tag{10}$$

The modeled transport equations for ε in the realizable k-ε   model is:

$$\frac{\partial}{\partial t}(\rho\varepsilon) + \frac{\partial}{\partial x_j}(\rho\varepsilon u_j) = \frac{\partial}{\partial x_j}[\ (\mu + \frac{\mu_t}{\sigma_\varepsilon})\frac{\partial\varepsilon}{\partial x_j}\ ] + \rho C_1 S\varepsilon - \rho C_2 \frac{\varepsilon^2}{k+\sqrt{v\varepsilon}} + C_{1\varepsilon}\frac{\varepsilon}{k}C_{3\varepsilon}C_b + S_\varepsilon \tag{11}$$

Here the S_ε and S_k are user-defined source terms.

G_k represents the generation of turbulence kinetic energy due to the mean velocity gradients.

G_b is the generation of turbulence kinetic energy due to buoyancy. In ANSYS Fluent, by default, the buoyancy effects on G_b are neglected simply by setting to zero in the transport equation for ε .

Y_M represents the contribution of the fluctuating dilatation in compressible turbulence to the overall dissipation rate, here the airflow is incompressible.

15

The degree to which is affected by the buoyancy is determined by the constant $C_{3\varepsilon}$. For buoyant shear layers that are perpendicular to the gravitational vector, $C_{3\varepsilon}$ will become zero.

Here the constants $C_{1\varepsilon}$=1.44, C_2=1.9, σ_k=1.0, σ_ε=1.2. The details of calculation of other parameters see in [4]

3.4. Enhanced Wall Treatment ε-Equation (EWT-ε)

The Enhanced Wall Treatment for the k-ε model is a near-wall modelling method, which combines a two layer model with so-called enhanced wall functions. The enhanced wall treatment can be defined to the traditional two-layer zonal model, when the near-wall mesh is fine enough to be able to resolve the viscous sublayer, that means typically the first near-wall node placed at $y^+ \approx 1$. However, the restriction that the near-wall mesh must be sufficiently fine everywhere might impose too large a computational requirement.

Ideally, it is better to have a near-wall formulation, which can be used with coarse meshes (usually referred to as wall-function meshes) as well as fine meshes. And additionally, for the intermediate meshes, which the first near-wall node is placed neither in the fully turbulent region nor in the direct vicinity of the wall at $y^+ \approx 1$, excessive error should not be incurred.

In order to achieve a near-wall modelling, it should possess the accuracy of the standard two-layer approach for fine near-wall meshes, simultaneously should not significantly reduce accuracy for wall-function meshes, ANSYS Fluent can combine the two-layer model with enhanced wall functions.

4. Model preparation

4.1. Spatial model

The geometry for CFD simulations can be obtained in two ways. One of them is to use the geometry directly, which is created numerically in the modelling software in ANSYS, such as SpaceClaim(SC) or Design Modeller. This method was extremely popular in the last decades. But the obvious disadvantage of this method is that the numerically model created in the CFD simulation software is incompatible with the file, which is created in CAD software, meanwhile the CAD software is the most commonly be used in the design field. Besides, creating of a model is quite difficult in the ANSYS software, if the model has complex geometry.

The other method is to use the file created in CAD software, which can be imported into the software tool (geometry preparation) in ANSYS directly. Some universal file formats (such as STEP) can be used. It can be done easier, therefore, this method is widely used currently.

In this work, the given geometry file of fan is also in the file format STEP, which can be imported not only into the modelling software as SC but also the geometry preparing software such as ANSYS Fluent Meshing

From the imported geometry of the fan Fig. 4 we can see that the casing of the fan is divided into numerous parts and the manufacturing particulars such as connect holes, edges on the inlet duct etc., but these manufacturing details make the numerical mesh unnecessarily difficult. In order to reduce the complexity of the numerical mesh creation, the geometry of the fan must be optimized.

In SC, the geometry was simplified and the undesired manufacturing details will be removed according to the following steps:

- all the holes were filled;
- all blades basis were removed and intersected with the rim;
- chamfer on the edges was removed;
- the overlapping geometry was joined;
- the empty space between inlet shape and the fan casing was filled;
- redraw the rounded casing according to the size of the original fan;

- The inlet was extended by 50 mm and outlet was extended by 250 mm in order to provide easier evaluation of fan inlet/outlet pressures.

The original geometry of fan and the optimized one are presented in Fig. 4 and Fig. 5. The Fig. 6 shows the cross section of the fan.
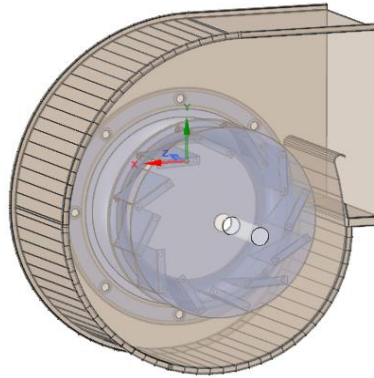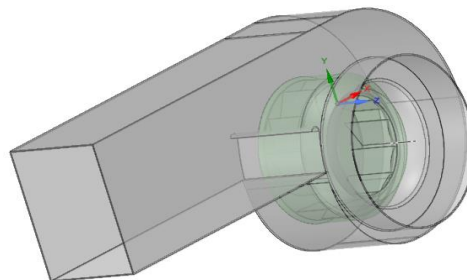

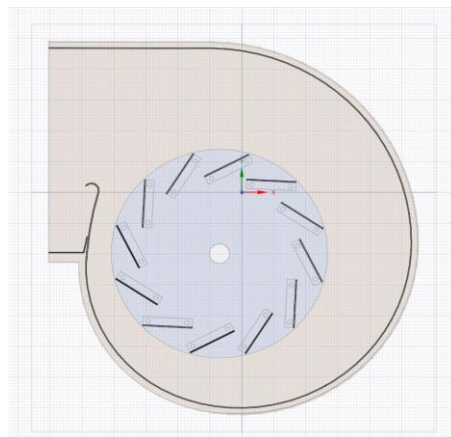Fig. 4 - Original geometry

Fig. 5 - Optimized geometry

Fig. 6 - Cross section of the fan

18

Additionally, in order to realize the MRF method, which is used in this work, a cylinder (the light green in Fig. 5) was created to enclose the rotated impeller of the fan. The cylinder is considered as the interface between stationary and moving frame.

4.2. Surfaces of the simplified geometry model

After simplifying and repairing the model, it is better to combine the individual components into fewer parts, therefore, it could be easier to analyze and also more convenient for the further work. In my work, all components were combined into three parts: fixed part, rotating part and cylindrical interface.

The goal of numerical model preparation is to create a volumetric mesh with large amount of finite control cells. The amount of cells of volume mesh is determined by the size of triangular surface mesh elements. If the mesh is overly fine, it requires more unnecessary computer memory demand, oppositely, the result of simulation will be inaccurate since the volume mesh is too rough i.e. too big mesh cells. Therefore, the surface mesh size from different components of fan should be variable according to the expected fluid velocity. In hence, surfaces of components should be defined with different names for the convenience of size field creating.

4.3. Computational mesh

4.3.1. Surface meshing

Size field creating

The volume mesh of model is obtainable by fulfilling the regions, which are enclosed within the base-object created surface mesh. In general, the most commonly used methods to create the surface mesh are Size Function Method and Scoped Sizing Method. In this work, the Scoped Sizing Method is chosen.

19

With the Scoped Sizing Method, not only an accurate sizing information of cells can be set for the mesh distribution, but also the precise refinement of surface mesh is realizable.

The velocity of fluid around the rotated surfaces of fan (impeller) is higher than the stationary surfaces, such casing, inlet, and so on. Therefore, smaller control size for rotated surfaces are set in comparison to the others. The Table 1 shows the sizes and types of each named components of fan.

Table 1 - Types and control sizes of size field for fan components

Name	Type	Control size (mm)
MRF (cylinder)	Hard	1
Blade surfaces and edges	Hard	0.5
Propeller back surfaces	Soft	1
Propeller back edges	Hard	0.3
Propeller front surfaces	Soft	1
Propeller front inside surfaces	Soft	1
Propeller front edges	Hard	0.3
Casing rounded	Hard	2
Casing outflow	Soft	5
Inlet connection	Soft	2
Inlet surfaces	Soft	2

Surface mesh

The scoped sizing definitions can be saved to a file (*.szcontrol). This file can be read in and reused for similar models if the sizing definitions should be changed. The size field was computed with desire dimensions and the generated size field was written in format of file ".sf ".

The first step to create the surface mesh was to import the simplified geometry simultaneously using the created size field. Each scoped field is defined separately with variable sizes. Therefore, all components were merged into one object named "fan". The further steps for obtaining of surface mesh with satisfied mesh quality are presented below.

(1) The inlet and outlet of the fan were patched

In order to achieve an enclosed volumetric regions for generating volume mesh, the inlet and outlet should be patched. In this step the "Patch Option" was used to create inlet and outlet labels, and these labels were added to the object i.e. fan. In addition, the type of both created patch labels should changed to "pressure inlet" and "pressure outlet" correspondingly.

(2) Surfaces in model were joined and intersected

The imaginary created cylindrical interface for MRF method intersects with surfaces of inlet duct. Therefore, the cross intersected surfaces from different components should be joined, in order to divide the hole fan chamber into three domains: inlet, cylinder and outlet. The function "Join/Intersect" realized this procedure in ANSYS Fluent.

(3) Surface mesh quality was improved

The quality of surface mesh influences the volume mesh quality, moreover, the simulation results. In hence, the surface mesh should be diagnosed and improved. The function "Diagnostics" provides respectively to check and improve the Face Connectivity and Quality of surface mesh.

Generally, the free faces, multiple faces, self-intersections and self-proximity from mesh cells should be repaired to improve the face connectivity. On the other hand, the mesh quality is improvable by controlling the skewness of mesh cells under the minimum value of 0.6. In this step the function "Diagnostics" was used to improve the quality of the surface mesh. Finally the improved surface mesh file was saved as a file in format "mesh" for the further using

4.3.2. Volumetric regions

Since the surface mesh based on the object was done, the volumetric regions were computed. There are six regions were computed in this model, and default type of region rims were all solid. The regions fulfilled with the air should change the type from solid to fluid. Furthermore, the name of created regions were also changed in order to better to recognize.

(i)   Firstly, the type of region which is enclosed in cylinder (except the solid rotated impeller) was changed from solid to fluid and renamed as cylinder.

(ii)   In the next step, the type of region which is enclosed between inlet surface and cylinder front surface was changed from solid to fluid and renamed as inlet.

(iii)   At last, the type of rest region which is enclosed in fan chamber was changed from solid to fluid and renamed as outlet.

The other entities such as rotated part and fixed part keep the type as solid. The computed volumetric regions are displayed in Fig. 7 below.
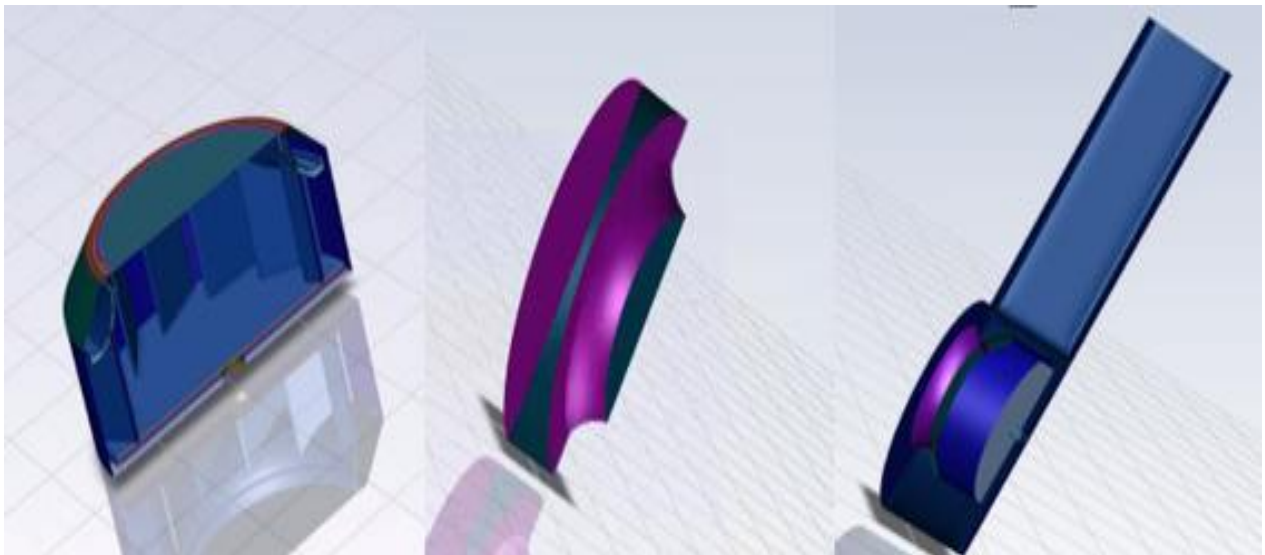
Fig. 7 - Cross section of cylinder/inlet/outlet (from left to right)

The volumetric mesh was generated by using of the volumetric regions. It is easy to generate the volume mesh using the function "Auto Mesh" in ANSYS Fluent.

It should be noted that this procedure for volume mesh generates a coarse mesh. In order to achieve the velocity field in the near wall regions where prismatic cell layers have to be set up. See in Fig. 8 how to set up the interface of "Auto Mesh"

Using the "Auto Mesh" interface, the "Keep Solid Cell Zones" was disabled. Because this is the coarse mesh procedure to achieve the parameters of the boundary mesh according to the coarse simulation, so "none" was chosen under the "Boundary Layer Mesh". The mesh cell type Poly-Hexcore to fill the volume was chosen and set 1 in both fields under "Buffer Layers" and "Peel Layers". Briefly, the quantity of generated mesh cells with type "Poly-Hexcore" is minimized due to the larger volume of single cell in comparison to the other types of cell. Besides, it is suitable for the geometry with high complexity.
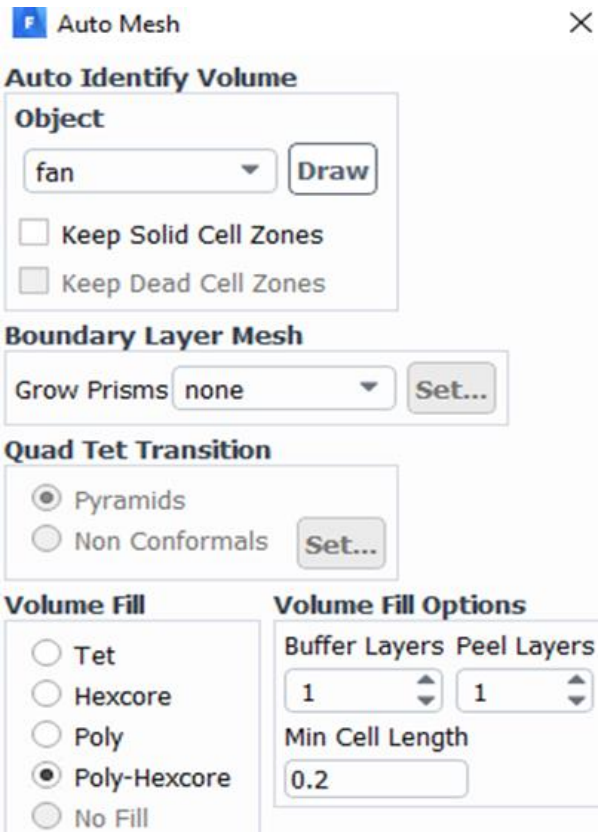
Fig. 8 - Interface of auto mesh

After the accomplishment of set up of the interface from "Auto Mesh", I generated the volumetric mesh of model by clicking the button "Mesh". Usually there are 3 indicators of mesh quality considered, they are the skewness, orthogonal quality and aspect ratio.

The mesh quality can be improved by function "Auto Node Move" if necessary. The indicators of generated coarse volume mesh are shown in Table 2. The values of indicators were in the acceptable range. The amount of generated volume mesh cells for coarse simulation was around 4.2 million.

Table 2 - Indicators of coarse mesh quality

Inverse Orthorgonal Quality			
name	cells (quality > 0.90)	maximum quality	cell count
inlet-poly-cells	0	0.67701483	172028
cylinder-poly-cells	0	0.79989172	3141752
outlet-poly-cells	0	0.79968079	928075
Skewness			
name	cells (quality > 0.90)	maximum quality	cell count
inlet-poly-cells	0	0.67701483	172028
cylinder-poly-cells	0	0.79989172	3141752
outlet-poly-cells	0	0.79968079	928075
Aspect Ratio			
name	minimum quality	maximum quality	cell count
inlet-poly-cells	1	7.8131755	172028
cylinder-poly-cells	1	32.936306	3141752
outlet-poly-cells	1	39.335996	928075

5. Coarse simulation

After accomplishing of the volumetric mesh, I've saved the volumetric mesh file and reopen the ANSYS Fluent in solution mode and setup the model in Fluent according to the following steps and conditions

5.1. Fluent Launcher

The Ansys Fluent was opened with 3D version and double precision. The parallel computing process was used and the maximum number of processes was set as 10. Generally, the single-precision solver provides commonly already the sufficient accuracy of simulation results for most cases. But the double-precision solver was chosen in this work in order to achieve more accurate results of the simulation.

5.2. Setup

In this work, the Realizable k-ε turbulence model was chosen, and the Near-Wall Treatment set as Enhanced Wall Treatment. The air with constant density 1.20 kg/m^3 and the dynamic viscosity was $1.815 \cdot 10^{-5}$ Pa·s was chosen for the fluid in this model. The air flow through the fan chamber was simulated as incompressible and without heat transfer. The energy equation was not considered as one of the governing equations.

5.3. Boundary conditions

The type of inlet was changed to pressure inlet with 0 pa static pressure and turbulence intensity 0.1 % and viscosity ratio 0.01. The type of outlet was changed to pressure outlet, the gauge pressure was 0 Pa and set the condition for backward flow with turbulence intensity 5 % and hydraulic diameter of the outlet $D_h = 0.162$m. Rotation was modelled by using the Multiple Reference Frame model (MRF). The speed of rotating part i.e. impeller was set to 2830 rpm. The rotating segments in the model were all the surfaces of the impeller enclosed by the "cylinder"

5.4. Solution setup

The Segregated solver was chosen, and the pressure-velocity coupling algorithm method SIMPLE was chosen. For solving the rotated machine was the PRESTO! (PREssure STaggering Option) scheme chosen for discretization of pressure equation. And for the other discretization second order upwind scheme was used. Then all of the discretization methods were set for second order. The default values of under-relaxation factors for each quantities were used to control the solution.

5.5. Results of the coarse simulation

The numerical model with all definitions can be saved in format named as CASE File. In the next step, the model was initialized by standard method and simulated for 8000 iterations for the coarse simulation. In the Fig. 9 shows the convergence of simulation represented by the residuals for each quantities.
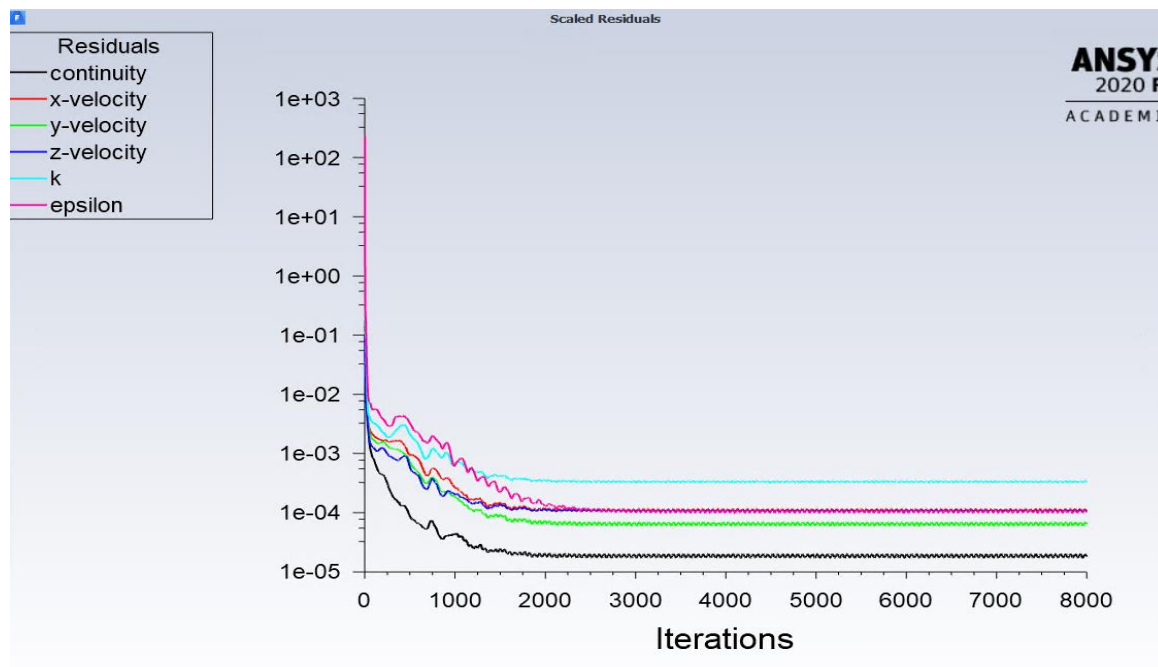
Fig. 9 - Residuals convergence for coarse simulation

The reason for the coarse mesh simulation was to check velocities near surfaces and adjust y^+ and y_1 values.

6. Determination of the parameters of prismatic layers

As the simulation of coarse model was completed, the values of wall shear stress from each component's surfaces of the fan could be read, thus the wall shear stress in variants of **Area-Weighted-Average**, **Facet-Maximum** and **Facet-Minimum** was evaluated.

The Area-Weighted-Average of a quantity (here the sheer stress) is computed by dividing the summation of the product (sheer stress) of the selected field variable and facet area by the total area of the surface, it can be calculated as the following equation:

$$\frac{1}{A}\int \tau_w \, dA = \frac{1}{A}\sum_{i=1}^{n} \tau_{wi} \, |A_i| \tag{12}$$

Where A is the total surface of each components;

A_i is the facet area of each cell;

τ_w is the total wall sheer stress on the surface of each components;

τ_{wi} is the wall sheer stress on the facet of each cell.

Facet-Maximum here is the maximum facet value of sheer stress on the component's surface, oppositely the Facet-Minimum is the minimum facet value of the sheer stress.

6.1. Calculation of the first prismatic layer height

The Enhanced Wall Treatment method is chosen for the near wall modelling. The Enhanced Wall Treatment behaves like the traditional two-layer zonal model, when the near-wall mesh is fine enough to be able to resolve the viscous sublayer, that means typically the first near-wall node placed at $y^+ \approx 1$.

The height of the first prism layer can be calculated using the following equations.

$$u_\tau = \sqrt{\frac{\tau_w}{\rho}} \tag{13}$$

$$y^+ = \frac{u_\tau \cdot \Delta y_1 \cdot \rho}{\mu} \tag{14}$$

u_τ $[\frac{m^2}{s}]$ is the friction velocity;

τ_w [Pa] is sheer stress at the wall;

ρ [kg/m^3] is the density and equals to 1.2;

μ [Pa·s] is the viscosity and equals to 1.815×10^{-5}.

If the dimensionless distance y^+ is set as 1, the calculated height of the first prism layer for each surfaces of fan are presented in Table 3. The values of wall sheer stresses of each fan components and more calculated details are in the Appendix.

Table 3 - The calculated height of first Layer from area weighted average/ facet maximum

Face Name	y_1_facet_max (mm)	y_1_area_average (mm)
baffle	0.013	0.040
blade-edges	0.006	0.019
blade-surfaces	0.008	0.019
casing-rounded	0.015	0.031
casing-sides	0.014	0.031
inlet-edge	0.013	0.018
inlet-surfaces	0.018	0.029
inlet-surfaces (27142)	0.009	0.015
inlet-surfaces (27143)	0.016	0.048
propeller-back-edge	0.013	0.020
propeller-back-surfaces	0.012	0.021
propeller-front-edges	0.010	0.015
peopeller-front-surfaces	0.009	0.021

6.2. Scoped prism file

The function "Auto Mesh" in ANSYS Fluent simplifies the procedure of creating the numerical model. Before generating the volume mesh, a scoped prism file for the boundary layer should be created according to the height of the first layer and the number of layers.

According to the calculated y_1 values over each component's surface of model from the coarse simulation, the prismatic layers were divided in five categories, such as propeller-outer- surfaces; propeller back outer surface; propeller inner surfaces and front edges; casing-rounded and inlet nuzzle and the other surfaces. The height of the first prismatic layer and the number of layer for each category were set as presented in Table 4.

Table 4 - Height of first prismatic layer and the number of layers

Scoped Surface Name	Scoped Prims List	first height (mm)	number of layers	total height (mm)
propeller-back-edge	propeller-outer-surfaces	0.02	14	1.183918
propeller-front-surfaces				
propeller-back-surfaces-outer	propeller back outer surface	0.03	14	1.775878
baffle-edge	casing-rounded and inlet nozzle	0.03	14	1.775878
baffle-rounded				
baffle-surface				
casing-rounded				
inlet-edge				
inlet-inner-surface				
inlet-outer-surface				
casing-flat outlet	other surfaces	0.5	7	6.457952
casing-sides				
blade-inner-edges	propeller inner surfaces and front edge	0.02	13	0.9699321
blade-outer-edges				
blade-surfaces				
propeller-back-surfaces-inner				
propeller-front-edges				

6.4. Volume mesh

The scoped size file of prismatic layers was used to generate the fine volume mesh in this step, and the procedures for fine volume mesh generating was similar as the procedures of the coarse volume mesh generating. But for this time, both the number of buffer layers and peel layers were set as 2 in order to achieve a smooth transition from prism layer to poly-hexcore cells.

As all the parameters were set, the volume mesh was generated using the "Auto Mesh" utility. The figures Fig. 10 and Fig. 11 present the model volume mesh.
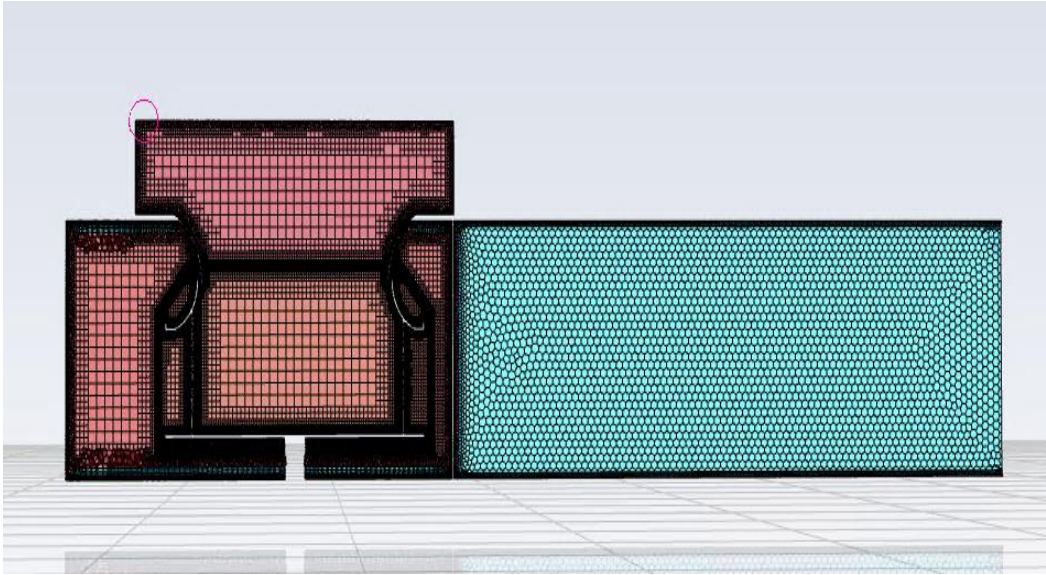
Fig. 10 - Cross section View of volume mesh with prismatic boundary layer on the selected surfaces

(A)   (B)
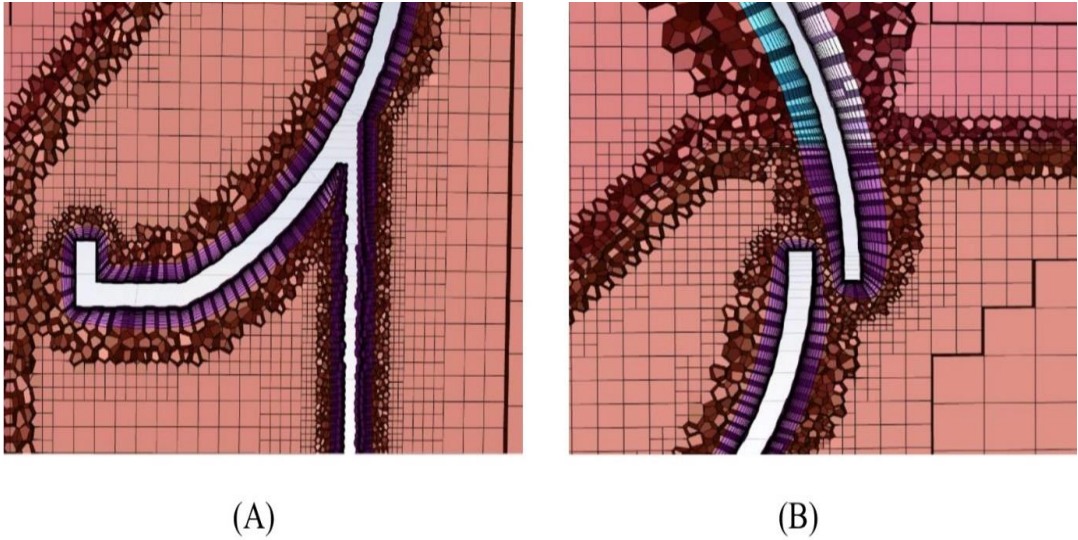
Fig. 11 - Detailed views of the prismatic boundary layer on (A) impeller front; (B) inlet nozzle (up) and the impeller front (down)

In the previous chapter it was presented that the total computational cells of the coarse mesh model (without boundary prismatic layers) was almost 4.2 million. But there were 15.7 million computational cells in total in the fine meshed model with the boundary prismatic layers.

6.3.1. Volume mesh improvement

After generating the volume mesh, the quality of mesh should be improved. If the mesh quality is not good enough, the residuals of the simulation will be difficult to converge.

In general, there are three significant indicators to evaluate the mesh quality:

- skewness
- orthogonal quality
- aspect ratio

The acceptable value ranges of indicators are shown in Table 5, additionally the aspect ratio should be smaller than 100.

Table 5 - Mesh quality recommendations

Skewness mesh metrics spectrum

Excellent	Very good	Good	Acceptable	Bad	Unacceptable
0-0.25	0.25-0.50	0.50-0.80	0.80-0.94	0.95-0.97	0.98-1.00

Orthogonal Quality mesh metrics spectrum

Unacceptable	Bad	Acceptable	Good	Very good	Excellent
0-0.001	0.001-0.14	0.15-0.20	0.20-0.69	0.70-0.95	0.95-1.00

Skewness

The skewness describes how close a face or cell is to the ideal equilateral triangle or equiangular quad. According to the definition of the skewness, the value of 0 means that the cell has the highest quality, while the value of 1 means the worst.

Using of the highly skewed faces and cells leads to a quality decreased the accuracy of results, so it is necessary to reduce the value of skewness of mesh i.e. to improve the mesh quality. The qualified value ranges are shown in the Table 5.

Orthogonal quality

The provided option for setting to control the Orthogonal Quality in Fluent ANSYS is the inverse Orthogonal Quality. The relation between Orthogonal Quality and Inverse Orthogonal Quality is obey the equation below:

$$\text{Inverse Orthogonal Quality} = 1 - \text{Quality} \qquad (15)$$

The following equations (16) and (17) are used to calculate the Inverse Orthogonal Quality. The maximum values of the results from equations below is the Inverse Orthogonal Quality for each cell.

$$1 - \frac{\vec{A_i} \cdot \vec{C_i}}{|\vec{A_i}| \; |\vec{C_i}|} \qquad (16)$$

$$1 - \frac{\vec{A_i} \cdot \vec{f_i}}{|\vec{A_i}| \; |\vec{f_i}|} \qquad (17)$$

$\vec{A_i}$ is the face normal vector for each face;

$\vec{C_i}$ is the vector from the cell centroid to the centroid of each of the adjacent cells;

$\vec{f_i}$ is the vector from the cell centroid to the centroid of each face.

Aspect Ratio

The Aspect Ratio is defined as the ratio of the longest edge length to the shortest edge length for a face or a cell. It applies to almost all shape types of the mesh cell, such as triangular, hexahedral, quadrilateral and tetrahedral elements. The Aspect Ratio can also be used to determine how close a face or a cell is to the ideal one. The Aspect Ratio is equal to 1 for an equilateral face or cell, and it will be greater than 1 for less regularly-shaped faces or cells.

It is important to check the skewness after improvement of the aspect ratio for the prisms. Because if there is a large jump of cell size between two cells then the skewness changed to its value, which can be out of the acceptable range.

The quality of volume mesh could be improved through the function "Auto Node Move" in ANSYS Fluent. The improved volumetric mesh can be saved as format MESH. File for the further use. The Table 6below presents the values of the three significant indicators of quality of the volume mesh as obtained for the fan model.

Table 6 - Significant indicators of quality of the volume mesh

Inverse Orthorgonal Quality			
name	cells (quality > 0.90)	maximum quality	cell count
outlet-prism-cells	0	0.89518241	1180545
inlet-prism-cells	0	0.31620366	208726
cylinder-prism-cells	0	0.89922271	7645926
inlet-poly-cells	0	0.79983731	362948
outlet-poly-cells	0	0.89420357	1634471
cylinder-poly-cells	0	0.89425651	4669179
Skewness			
name	cells (quality > 0.90)	maximum quality	cell count
outlet-prism-cells	0	0.89518241	1180545
inlet-prism-cells	0	0.31620366	208726
cylinder-prism-cells	0	0.89922271	7645926
inlet-poly-cells	0	0.79983731	362948
outlet-poly-cells	0	0.89420357	1634471
cylinder-poly-cells	0	0.89425651	4669179
Aspect Ratio			
name	minimum quality	maximum quality	cell count
outlet-prism-cells	1.6550446	98.877259	1180545
inlet-prism-cells	2.4546151	92.728308	208726
cylinder-prism-cells	2.0583628	98.957758	7645926
inlet-poly-cells	1	13.855676	362948
outlet-poly-cells	1	77.111855	1634471
cylinder-poly-cells	1	96.293598	4669179

As described in the chapter 6.2, the model of fan is divided into three volumetric regions: inlet, outlet and the cylinder. Therefore, the fine volume mesh of the model is divided into six mesh cell zones, which are listed in Table 6 above. The boundary prismatic layer on the element's surfaces and simultaneously enclosed in the region outlet is named as "outlet-prism-cells". The poly-hexcore cells, which are filled in the region outlet (except the boundary layers) are named as "outlet-poly-cells".

7. Numerical solution

In this project, five operational points were simulated based on five different values of gauge pressure were set at the model outlet, which were 0 Pa, 100 Pa, 200 Pa, 300 Pa and 350 Pa. These gauge pressures set at the model outlet represent various pressure losses of a virtual duct system which would be connected to the fan. The difference between total pressures at the fan inlet/outlet was evaluated for each setup described above. The evaluated fan total pressures were combined with the evaluated air flowrates to obtain performance curve, i.e. the P-V curve.

The gauge pressure is defined as the difference between the absolute pressure and the atmospheric pressure. In other words, if the gauge pressure is set to 0 Pa, it means that the absolute pressure at the outlet of model is equal to the atmospheric pressure.

In the beginning of the procedure of this project, the outlet and the inlet of the fan has been extended in SpaceClaim (SC). Therefore, cut-planes were created in Fluent ANSYS, where the original outlet and inlet of the fan are positioned. The positions of the fan outlet and inlet can be read in the model in SC, and these positions can be set in Fluent. The Fig. 12 illustrates the position of two outlets denoted as "model" and "fan".
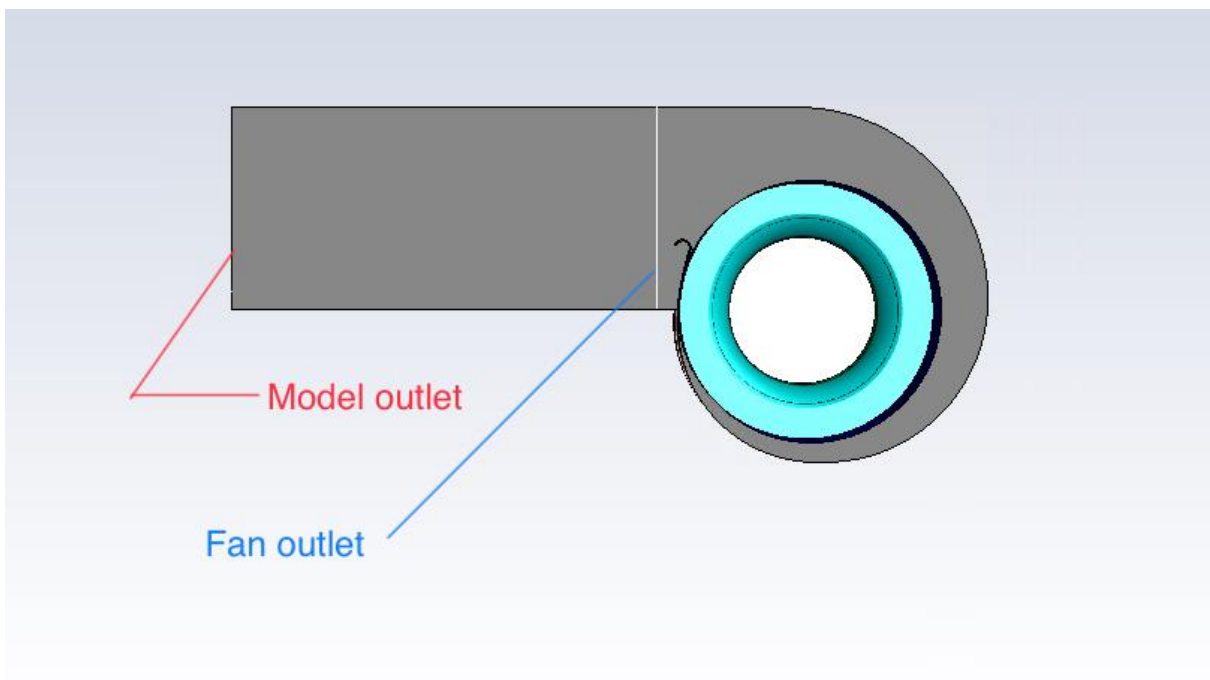
Fig. 12 - Model outlet and fan outlet

All the simulations were performed with the density of air 1.2 kg/m^3 and dynamic viscosity 1.815x 10^{-5} Pa.s.

The MRF method for the rotating impeller was chosen in this work. All rotated components of the fan were enclosed in an imaginary cylindrical interface, which is in the current model named "cylinder". The type of motion for all rotated components was changed to "rotational". The speed of the impeller was set to 2830 rpm.

7.1. Simulation convergence

The residuals of quantities (such as velocities, continuity, turbulent kinetic, and so on) were used as monitor to control the simulation convergence.

In order to achieve developed turbulent airflow, I started with the First Order Upwind method for the momentum discretization and run the simulation for around 500 iterations. Then I changed the momentum discretization method to Second Order Upwind, and run about 10000 iterations to obtain fully developed airflow. The Fig. 13 shows the contour of velocity magnitude in fan with fully developed flow.
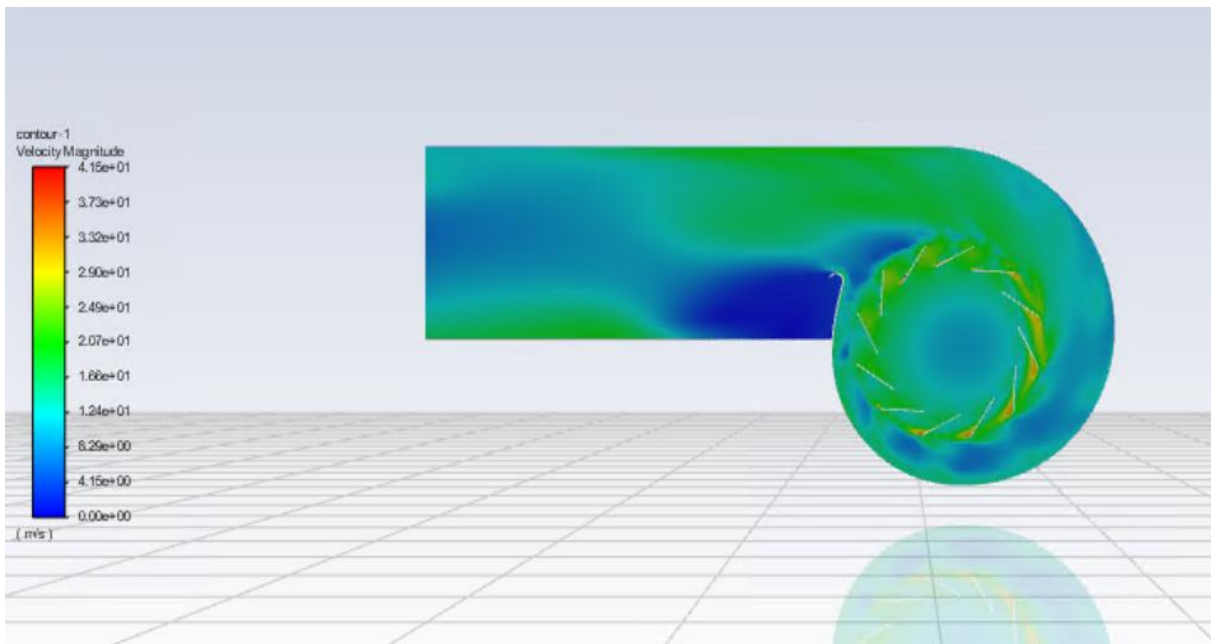
Fig. 13 - Contour of velocity magnitude in fan

Fig. 14 shows the convergence of simulations based on the residuals. The residual graph presented the residuals with gauge pressure 0 Pa at the model outlet.

When the gauge pressure of outlet increased, the simulation is harder to convergence. The solution in this situation is to increase the under-relaxation factor of pressure and decrease the under-relaxation factor of momentum. As shown in Fig. 14, the residuals of continuity dropped continued to stability.
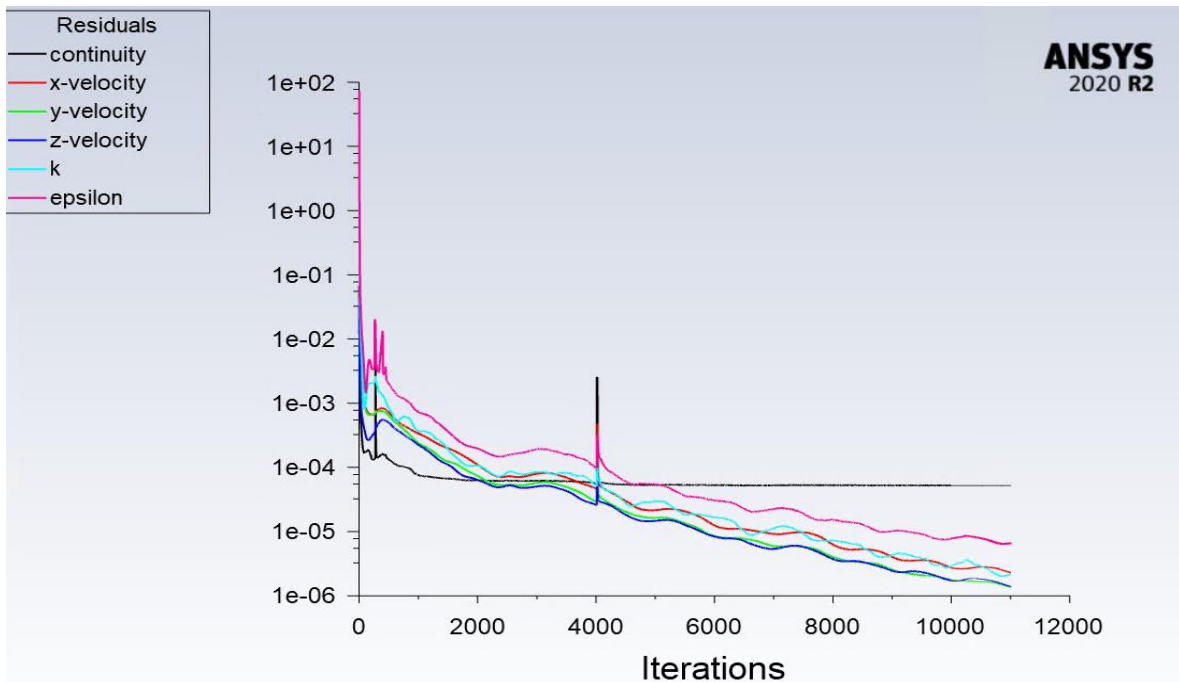
Fig. 14 - Residuals convergence for gauge pressure 0 Pa

From the Fig. 14 we see that the value of residuals for continuity equation was less than 10^{-4}, for other equations the value of residuals were less than 10^{-4}. It fitted the criterion of convergence. Thus the simulation of model with gauge pressure 0 Pa was considered as converged. The simulation for other gauge pressures as 100 Pa, 200 Pa, 300 Pa and 350 Pa were also simulated with the same criterions of convergence.

7.2. Static pressure and velocity field

A plane positioned at the location of fan outlet was created for the evaluation of fan total pressure. It is shown as thin black line on the following figures, just across the extended outlet duct behind the scroll baffle of the fan.
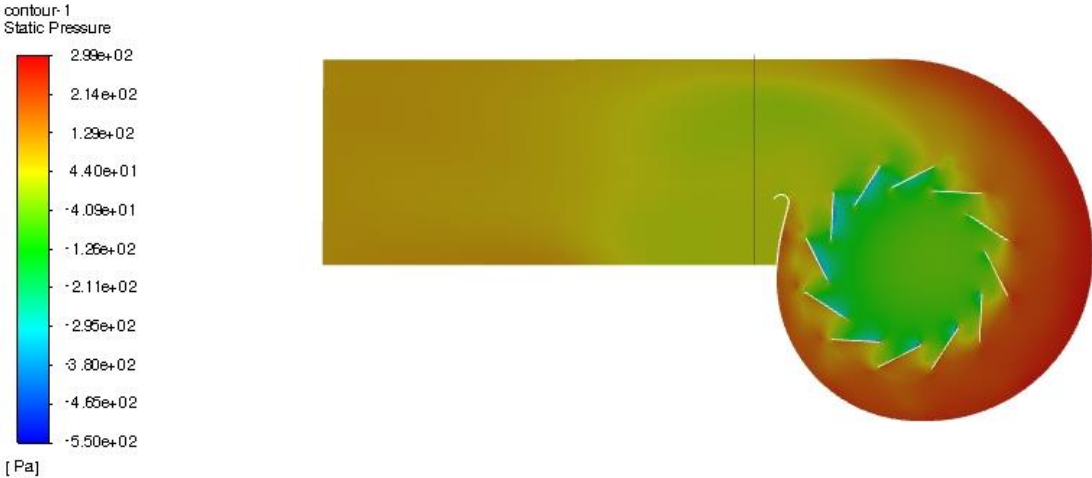
37
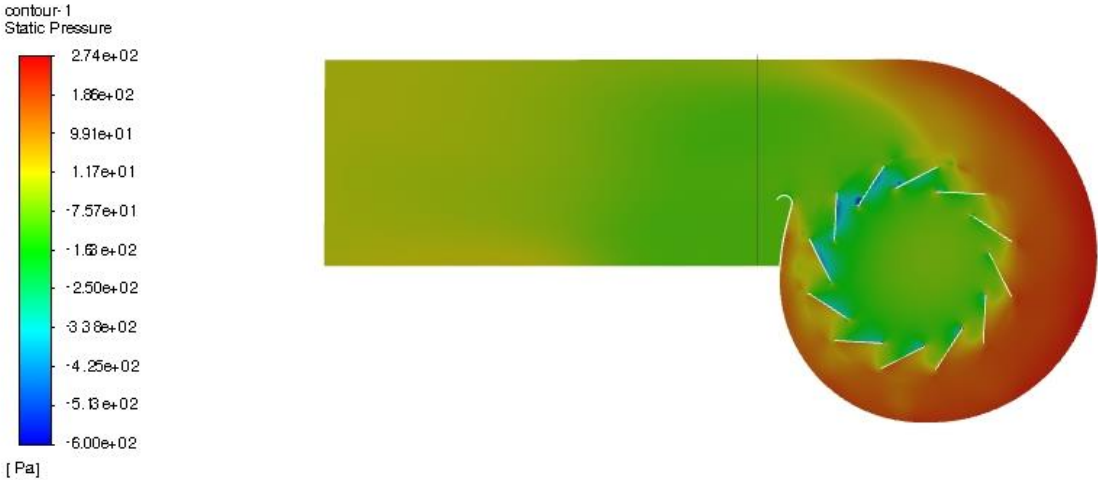
Gauge pressure = 0 Pa

Fig. 15 - Contour of static pressure in the fan chamber for gauge pressure 0 Pa
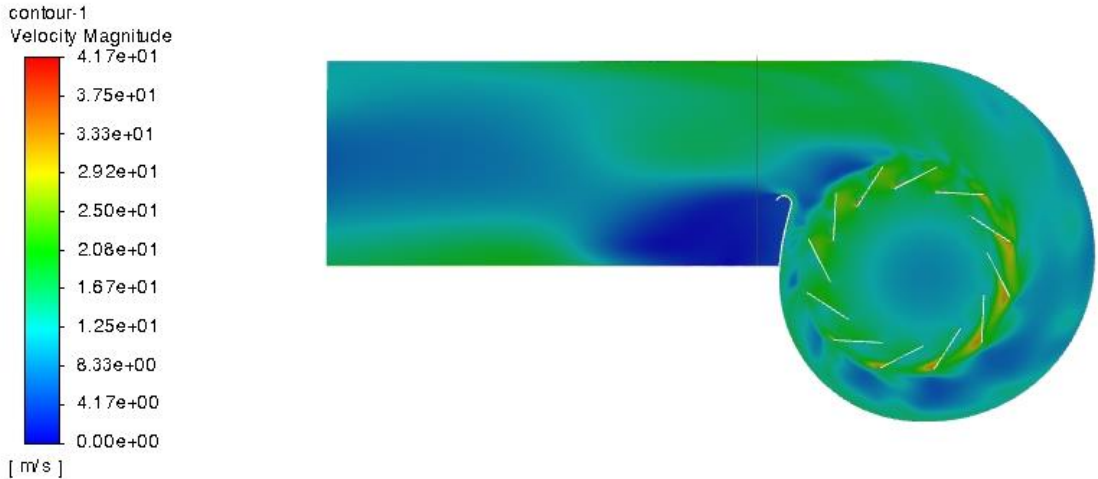
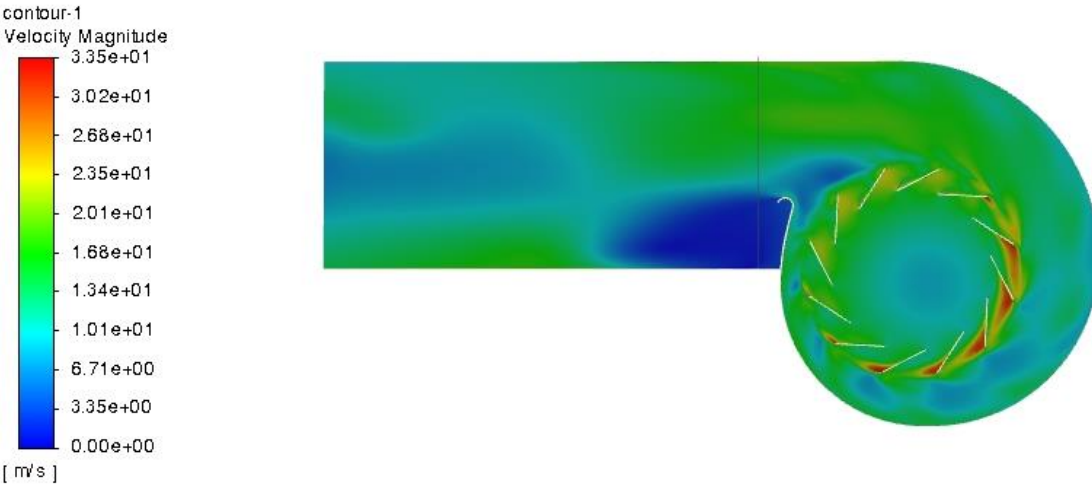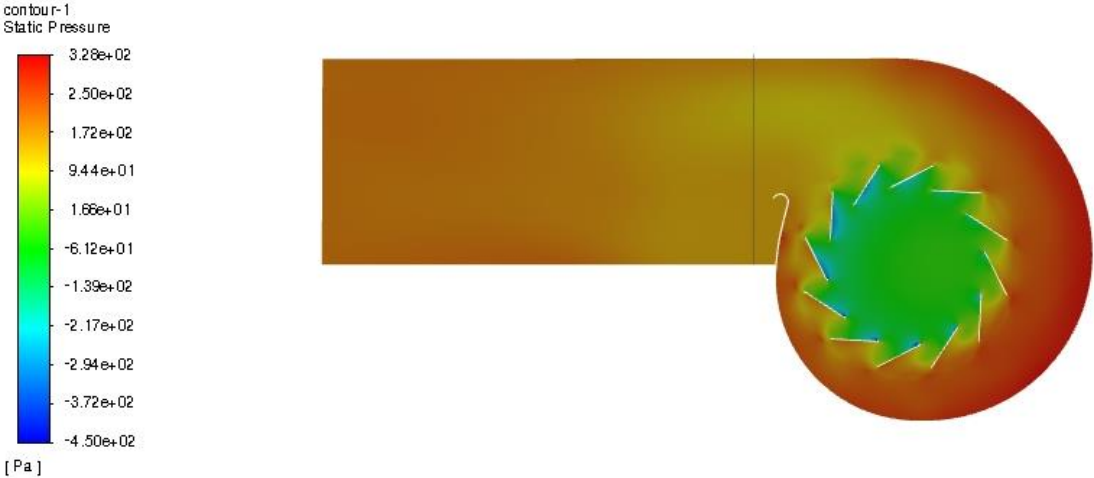Fig. 16 - Velocity magnitude in the fan chamber for gauge pressure 0 Pa

From the Fig. 15 we can see that the static pressure in the region inside the impeller is around -100 Pa, the lowest static pressure occurs behind the blades and the value of this lowest static pressure is probably -600 Pa. The static pressure in the region outside of the impeller increases counterlockwise along the fan casing, then decreases when approaching the fan outlet. The highest static pressure in the fan chamber for the 0 Pa gauge pressure of the outlet is approximately 280 Pa.

38

It's worth noting that the static pressure at the outlet of the fan (position where the black line is) is lower than at the model outlet. The static pressure at the model outlet is approximately equal to the set gauge pressure, but the static pressure of the fan outlet is negative, the value is around -10 Pa.

From the Fig. 16 we can see that in the region inside of impeller, the airflow velocity is around 10 m/s, it presents the velocity of sucked airflow. The velocity of airflow is increased rapidly in the column between blades, it's almost 23 m/s. the highest velocity of the airflow appears behind the blades counterlockwise in direction four o'clock, which has around 40 m/s.

The airflow velocity in the upper part of the fan outlet is higher than in the lower part. It is equal to 0 in the region behind the scroll baffle. The airflow velocity in the upstream of the fan outlet is around 20 m/s.
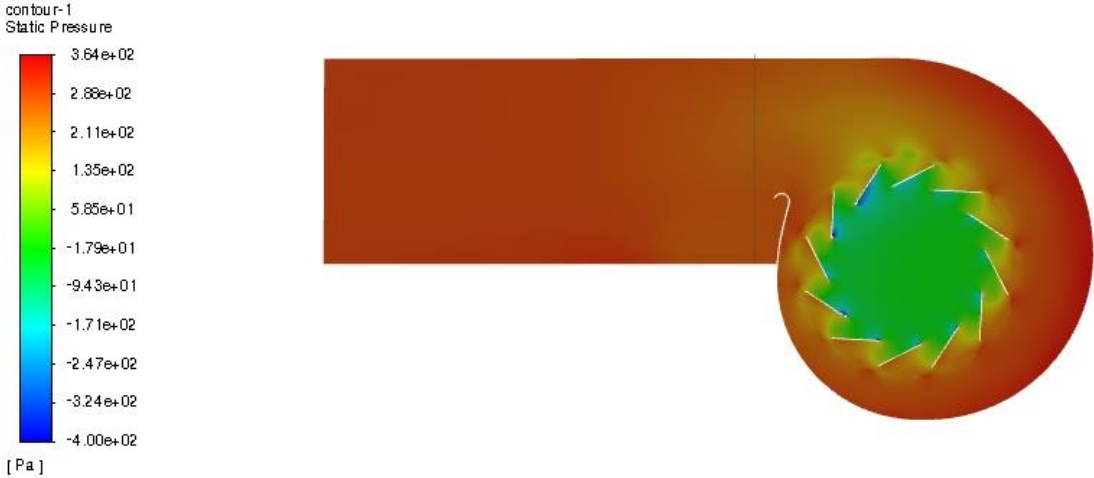
Gauge pressure = 100 Pa

Fig. 17 - Contour of static pressure in the fan chamber for gauge pressure 100 Pa

Fig. 18 - Velocity magnitude in the fan chamber for gauge pressure 100 Pa

The distributions of the static pressure and velocity magnitude in fan chamber are quite similar to the previous operational point, only the highest pressure increases to around 300 Pa and the lowest static pressure is decreased 50 Pa.

The maximum airflow velocity of the operational point is decreased from 41.7 m/s to 33.5 m/s. But it also can be seen that the magnitude of airflow velocity behind the blades i.e. in the column between blades is increased.

40

Gauge pressure = 200 Pa

Fig. 19 - Contour of static pressure in the fan chamber for gauge pressure 200 Pa
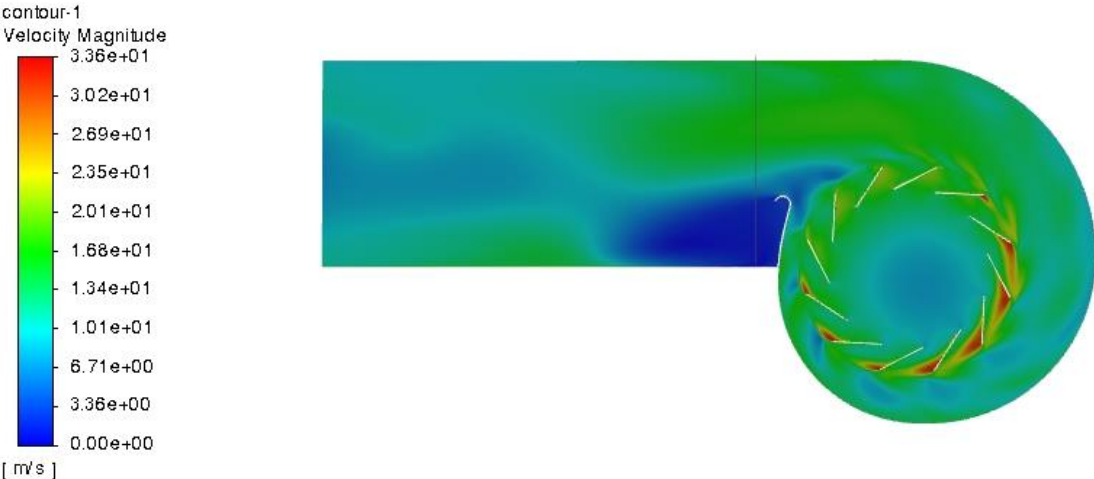
Fig. 20 - Velocity magnitude in the fan chamber for gauge pressure 200 Pa

Gauge pressure = 300 Pa

Fig. 21 - Contour of static pressure in the fan chamber for gauge pressure 300 Pa
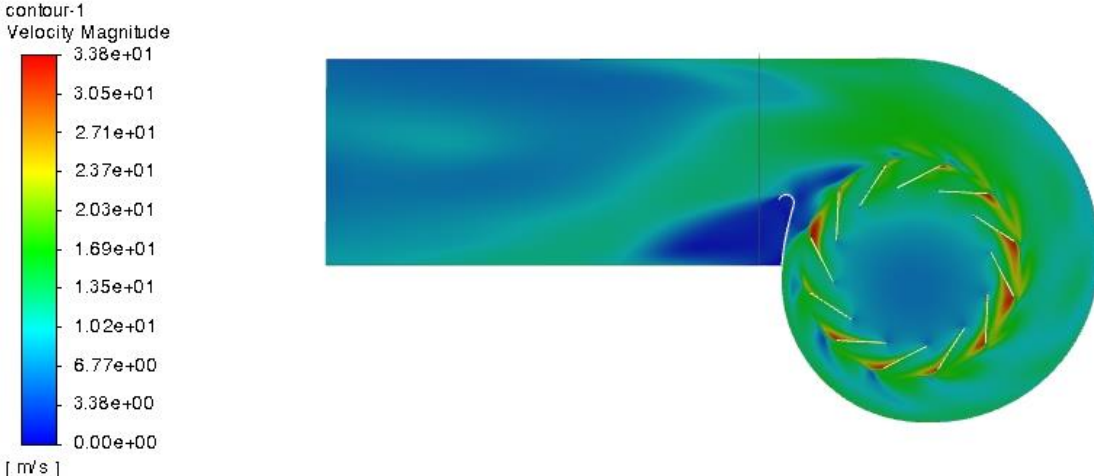
Fig. 22 - Velocity magnitude in the fan chamber for gauge pressure 300 Pa

Gauge pressure = 350 Pa

Fig. 23 - Contour of static pressure in the fan chamber for gauge pressure 350 Pa
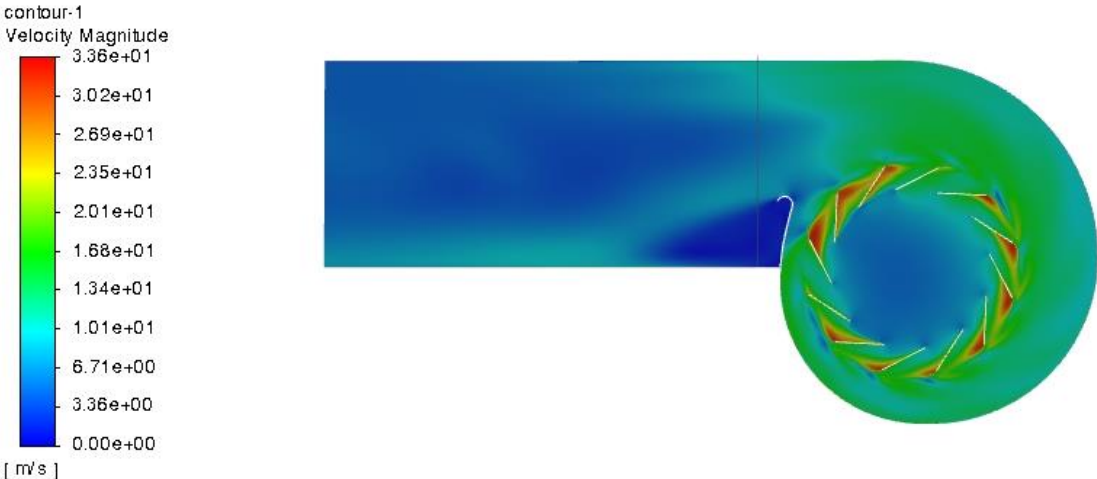
Fig. 24 - Velocity magnitude in the fan chamber for gauge pressure 350 Pa

The static pressure and velocity magnitude fields for the operational points defined by gauge pressure 200 Pa are similar to the previous setups. But for the gauge pressures 300 Pa and 350 Pa make some differences. We can see that the static pressures in the region of extended duct are nearly equal or even higher than the set boundary condition gauge pressure.

The airflow velocities on the model outlet of the operational points for gauge pressures 300 Pa and 350 Pa are lower. For the gauge pressure 300, the airflow velocities on the model outlet are around 7 m/s. And for the gauge pressure 350 Pa. they are even lower than 3.5 m/s.

7.3. Performance curve

The simulated results at the fan inlet and outlet were read from the Fluent as shown Table 7 below. In order to achieve the P-V Curve of the fan, the pressure differences between the total pressure of the fan outlet and inlet were calculated, and the calculated results are shown in the Table 7 in term "Fan total pressure".

Table 7 - Total pressures and flowrates

	inlet		outlet		
Gauge pressure (Pa)	Volume flow rate (m3/s)	Total pressure (Pa)	Volume flow rate (m3/s)	Total pressure (Pa)	Fan total pressure (Pa)
0	0.3050	1.0	0.3054	65.8	66.7
100	0.2809	0.8	0.2812	152.9	153.8
200	0.2529	0.7	0.2531	243.5	244.2
300	0.2027	0.5	0.2028	328.9	329.4
350	0.1652	0.4	0.1652	367.9	368.3

The diagram of simulated performance curve of the fan relates to the flowrate and overall total pressure is presented in the Fig. 25.
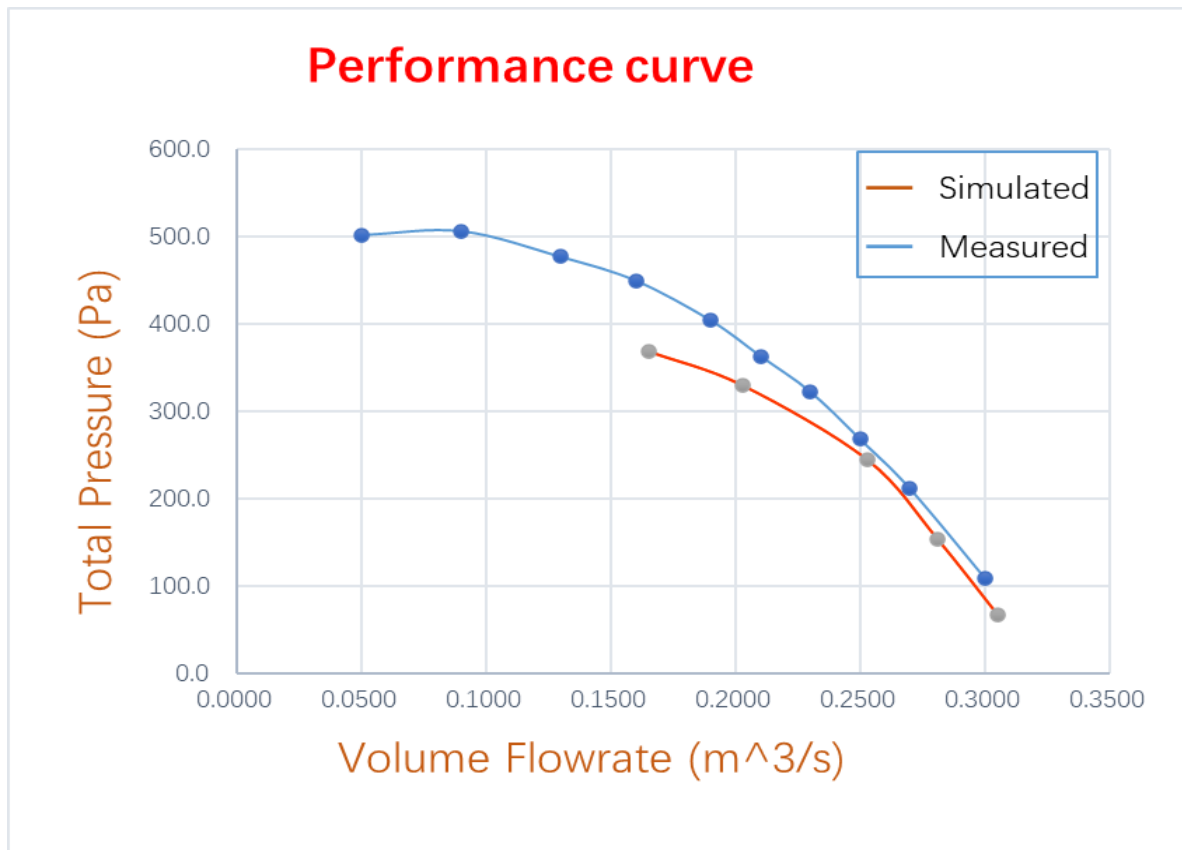
Fig. 25 - Comparison of the P-V curve between simulated and measured data
Measured data provided by ALTEKO.

The Fig. 25 shows that up to approximately 250 Pa of the total pressure, the two curves are very close each to other. But as the gauge pressure which was set at the model outlet is above 200 Pa, the simulated performance curve is lower than the measured curve.

From the Fig. 25 we can see that the fan volume flowrate is decreased with the increasing fan total pressure. The experimental curve shows that the maximum working pressure of this fan is around 500 Pa, but the maximum simulated value is around 400 Pa.

The reason for the deviation between measured and simulated curve can be that the simulation was not totally converged, because form the Table 7 we can see that the flowrate through inlet and outlet were not exactly equal. After the calculation, we know that the maximum deviation of the flowrates is 0.14%, but the differences of the total pressure between measured curve and simulated curve at the higher gauge pressure setup are more than

100 Pa, therefore, the convergence of simulation in this work influences the results not much. It should be noted that it was hard to converge the model for high gauge pressures at the model outlet.

Besides, the mesh quality of model also could lead to the deviation of simulated results. As described in previous procedures, the mesh quality of some mesh cell regions were only in the acceptable range, thus the mesh quality improvement could be one of the method to decrease the deviation between measured curve and simulated curve.

8. Conclusions

The goal of this project was to use the Multiple Reference Frame (MRF) method available in ANSYS Fluent to simulate the model with the geometry based on the centrifugal fan type RFE200-L produced by ALTEKO. The results of CFD simulations with the created model were then compared to the measured fan performance curve provided by ALTEKO.

The thesis provides information about the methodology of the geometry preparation and the numerical meshing for the CFD simulation of a centrifugal fan. The individual procedures of CFD simulation with MRF method were discussed in detail, including geometry preparation, creation of numerical mesh, CFD simulation and results evaluation. The relevant theoretical knowledge was also presented in the introductory part of the thesis.

This study was based on the geometry of the RFE200-L centrifugal fan created in SolidWorks by ALTEKO. The geometry was imported into ANSYS SpaceClaim, then it was optimized and simplified for the CFD simulations. A triangular surface mesh was created in ANSYS Fluent Meshing based on the fan surface geometry. Subsequently, the polyhedral volumetric mesh was generated with prismatic cell layers in the near wall regions. A coarse simulation was performed to determine the parameters of the prismatic cell layers. The CFD simulation of airflow in fan with rotating impeller was done in ANSYS Fluent for five operating points and the results were evaluated in terms of the fan performance curve.

From the comparison between the fan performance curve obtained from simulated data and the measured curve provided by ALTEKO, we can see that the deviation between simulated results and measured results are small when the fan total pressures are lower than 250 Pa. When the total pressure is higher than 250 Pa, the simulated results are substantially lower than the measured results.

The reason for the deviation between the simulated and measured P-V data could be the quality of numerical mesh. The values of indicators of mesh quality were only in the acceptable range for some mesh cell zones. Therefore, the mesh quality could be improved further to obtain more accurate simulation results. It was also found out that the convergence of simulation was difficult to achieve for gauge pressures at the model outlet which were 300 or 350 Pa. The reason for this might be again the quality of numerical mesh.

Another subject of further research could be the straight piece of duct connected to the fan outlet. This extension is used in order to avoid measurements in complex and disturbed flow which occurs just behind the fan outlet. However, in CFD simulations this extension might not be necessary. Whether the straight duct extension is needed or not in simulations, can be tested on models with different duct length (including the case without any duct).

References

[1] 2000 HAVC System and Equipment. Chapter 18, Fans, 2000

[2] Yu J.F, Qian J.M, Centrifugal Fan, in Electrical Motor Products, 2011

[3] Versteeg H.K., and Malalasekera W., Malaysia: Longman Group Ltd, 1995

[4] ANSYS Inc. Ansys Fluent Fluent User's Guide. USA: ANSYS Inc., 2013.

[5] Zelenský P., Barták M., Zavřel V., Zmrhal V. and Krupa R., Numerical Analysis of Air Flow in a Modular Fan Unit Using CFD Simulation. E3S Web of Conferences 111, Prag, Czech Republic, 2019.

[6] Gullberg P., Sengupta R., Axial Fan Performance Predictions in CFD, Comparison of MRF and Sliding Mesh with Experiments, In: Proceeding of the 11th European Conference on Turbomachinery Fluid Dynamics and Thermodynamics, Istanbul, Turkey, 2011.

[7] Jousef M.,"What is y^+ (yplus)?", SimScale CAE Forum,(2008), links to: https://www.simscale.com/forum/t/what-is-y-yplus/82394

[8] Singh O.P., Khilwani R., Sreenivasulu T., Kannan M., PARAMETRIC STUDY OF CENTRIFUGAL FAN PERFORMANCE: EXPERIMENTS AND NUMERICAL SIMULATION, International Journal of Advances in Engineering & Technology, May 2011.

[9] Huang CH.K., Hsieh M.E., Performance Analysis and Optimized Design of Backward-Curved Airfoil Centrifugal Blowers, February 15, 2009.

[10] Luo J. Y., Issa R. I., and Gosman A. D.. "Prediction of Impeller-Induced Flows in Mixing Vessels Using Multiple Frames of Reference". In IChemE Symposium Series. 136. 549–556. 1994.

[11] Launder B.E., Spalding D.B., The numerical computation of turbulent flows. Computer Methods in Applied Mechanics and Energy, no. 3, pp. 269–289, 1974.

[12] Yakhot V., Orszag S.A., Renormalization group analysis of turbulence. Journal of Scientific Computing, vol. 1, pp. 3–51, 1986.

[13] Shih T., Liou W., A., Shabbir Z. Yang, J. Zhu, A new eddy viscosity model for high Reynolds number turbulent flows. Computers & Fluids, vol. 24, pp. 227–238, 1995.

[14] Muhammad A., Numerical analysis of friction factor for a fully developed turbulent flow using keε turbulence model with enhanced wall treatment, School of Chemical & Materials Engineering, National University of Sciences & Technology, Islamabad ,Pakistan, 2014

[15] Mesh Quality & Advanced Topics, lecture 7 from Introduction to ANSYS Meshing, ANSYS, Inc. February 12, 2015

List of figures

List of tables

Appendix

	Wall sheer stresses			Friction velocities		Calculated height of first prismatic layer	
Face Name	Area-weighted-Average (Pa)	Facet-Maximum (Pa)	Facet-Average (Pa)	ut_facet_max (m/s)	ut_area_average (m/s)	Y1_facet_max (mm)	Y1_area_average (mm)
baffle	0.671	6.809	0.695	2.382	0.748	0.013	0.040
blade-edges	3.204	29.215	4.239	4.934	1.634	0.006	0.019
blade-surfaces	3.003	18.457	3.196	3.922	1.582	0.008	0.019
casing-rounded	1.123	4.730	1.186	1.985	0.968	0.015	0.031
casing-sides	1.116	5.705	1.132	2.180	0.964	0.014	0.031
inlet-edge	3.400	6.861	3.401	2.391	1.683	0.013	0.018
inlet-surfaces	1.346	3.446	1.375	1.695	1.059	0.018	0.029
inlet-surfaces27142	5.180	12.584	5.064	3.238	2.078	0.009	0.015
inlet-surfaces27143	0.478	4.193	0.577	1.869	0.631	0.016	0.048
propeller-back-edge	2.795	6.897	2.877	2.397	1.526	0.013	0.020
propeller-back-surfaces	2.413	7.824	2.476	2.553	1.418	0.012	0.021
propeller-front-edges	4.723	11.501	4.720	3.096	1.984	0.010	0.015
peopeller-front-surfaces	2.605	13.582	2.610	3.364	1.473	0.009	0.021
propeller-shift	1.689	4.131	1.670	1.855	1.186	0.016	0.026